

# **Investigations into the Operation of Diamond Microplasma Devices for Use at Atmospheric Pressure and Above**

**Samantha Vincent**

Supervisor: Professor P. W. May

Second Assessor: Dr. N. Fox

**2013**



A thesis submitted towards the fulfilment of the requirements for the honours  
degree of Bachelor of Science in Chemical Physics

## Abstract

This thesis reports the investigation into the fabrication and operation of microplasma devices offering stable discharges at atmospheric pressure and above. Work during the project built on that of the Bristol CVD laboratory into fabricating and operating microplasma devices based on microcrystalline diamond wafers.

The motivation for the project stemmed from the increased functionality that would be offered should operation of microplasma arrays be stable at high pressure (above atmospheric). Longevity of microplasma devices is also an important consideration, and as such research into diamond based devices offers promise for commercial viability.

Successful operation of a diamond based microplasma in a helium atmosphere at pressures from 33 kPa to 132 kPa was achieved for over 6 hours. The device featured thin film gold electrodes, with a cavity of 200  $\mu\text{m}$  and an electrode separation of 80  $\mu\text{m}$ . A glow which was characteristic of the abnormal glow mode was observed, and electrical characteristics were as expected. Several similar devices were fabricated with smaller diameter cavities, however some setbacks arose which meant it was not possible to test these devices within the time constraints of the project.

A device fabricated<sup>1</sup> in the Bristol CVD laboratory was tested and a discharge successfully struck. The device was based on a diamond substrate, with boron-doped layers of CVD diamond on both sides and U-shaped copper contacts. The discharge was slightly unstable and was removed for cleaning before further testing.

Three further devices featuring a boron-doped diamond layer were also fabricated using a hot filament CVD process. Due to time constraints of the project, these devices need modification before testing in the high pressure chamber.

---

<sup>1</sup> The device was fabricated by Monika Zeleznik, as part of the work towards a PhD in the University of Bristol Diamond Laboratory

# Table of Contents

<b>1</b>	<b>Introduction</b>	<b>4</b>
<b>1.1</b>	<b>Introduction to Plasmas</b>	<b>4</b>
1.1.1	Properties and Behaviour of Plasmas	4
1.1.2	Density	4
1.1.3	Temperature	4
1.1.4	Energy Distribution	5
1.1.5	The Debye Length and Mean Free Path	6
1.1.6	Existence of Plasmas	8
<b>1.2</b>	<b>Gas Discharge Plasmas and the Hollow Cathode Discharge</b>	<b>9</b>
1.2.1	Gas Discharge Plasmas	9
1.2.2	Regions of a gas discharge	10
<b>1.3</b>	<b>The Hollow Cathode Discharge</b>	<b>13</b>
1.3.1	Introduction to the Hollow Cathode Discharge	13
1.3.2	Modes of the Hollow Cathode Discharge	14
<b>1.4</b>	<b>High Pressure Discharges</b>	<b>16</b>
1.4.1	Paschen Law and Breakdown Voltage	16
1.4.2	The $pD$ Scaling Law	17
<b>1.5</b>	<b>Microplasmas</b>	<b>19</b>
1.5.1	Introduction to Microplasmas	19
1.5.2	Ion and Electron Kinetics in Microplasma Devices	20
1.5.3	Instabilities	21
1.5.4	The Breakdown of the Paschen Curve	22
1.5.5	Optical properties and modes of discharges	23
1.5.6	Materials and Fabrication	27
1.5.7	Applications	28
<b>1.6</b>	<b>The Use of Diamond in Microplasmas</b>	<b>30</b>
1.6.1	Introduction	30
1.6.2	Properties of Diamond	30
1.6.3	Doping Diamond	31
<b>2</b>	<b>Experimental</b>	<b>34</b>
<b>2.1</b>	<b>Fabrication of the Devices</b>	<b>34</b>
2.1.1	The Diamond Substrate	34
2.1.2	Electrode Deposition	36
2.1.3	Laser Drilling	37
2.1.4	Cleaning of Devices	38
2.1.5	Electrical Contacts	38
<b>2.2</b>	<b>The High-Pressure Chamber</b>	<b>40</b>

<b>2.3</b>	<b>Operation</b>	<b>41</b>
<b>3</b>	<b>Results and discussion</b>	<b>42</b>
<b>3.1</b>	<b>Overview</b>	<b>42</b>
<b>3.2</b>	<b>Operation of Boron-doped Sample</b>	<b>42</b>
<b>3.3</b>	<b>Operation of Metal Electrode Sample</b>	<b>43</b>
3.3.1	Electrical Characteristics	44
3.3.2	Optical Characteristics	46
<b>4</b>	<b>Afterword</b>	<b>49</b>
<b>4.1</b>	<b>Conclusion</b>	<b>49</b>
<b>4.2</b>	<b>Future Work</b>	<b>50</b>
<b>4.3</b>	<b>Acknowledgements</b>	<b>51</b>
<b>5</b>	<b>References</b>	<b>52</b>
	<b>Appendix</b>	<b>55</b>

# 1 Introduction

## 1.1 Introduction to Plasmas

A plasma is a collection of electrons and ions, with an overall neutral charge. Energy must be supplied to remove electrons from their atoms, and must be sustained in order to prevent the ions and electrons recombining. A distinctive characteristic of a plasma is that the kinetic energy of particles must be greater than the electrostatic energy between the particles. This distinguishes plasmas from other matter where short-range electrostatic interactions play a prominent role in a matter's characteristics. Plasmas are not commonly occurring on Earth due to its low temperature and high pressure relative to the conditions required for plasma formation. It is, however, thought that the majority of visible matter in the universe is in the plasma state.

### 1.1.1 Properties and Behaviour of Plasmas

Plasmas are more complicated to model than other matter due to the presence of charged particles and therefore the influence of electromagnetic forces. The three most fundamental parameters are density  $n$ , temperature  $T$ , and the magnetic field  $B$ . Other parameters, such as pressure, may be derived from these three parameters [1].

### 1.1.2 Density

The properties of individual plasmas are influenced by not only the overall particle density  $n$ , but the density of the charged species. Electrons and ions respond differently to electric and magnetic fields and must therefore be treated separately. Plasmas are not only influenced by the Earth's electromagnetic fields but by those created within the plasma. The potential difference between the electrons and positive ions creates an electric field. In addition, the movement of the charged particles creates a magnetic field, which in turn produces an electric field. In this way, the motion of all particles is interconnected. In stable plasmas, the density of positively and negatively charged particles is approximately equal, giving an overall charge neutrality. For a plasma to maintain its state, any deviation of charge neutrality must be small [2].

### 1.1.3 Temperature

Plasmas may exist over a range of temperatures, depending on the conditions in which the plasma exists. Some of the hottest plasmas have temperatures to the order of  $10^6$  K and exist in the centre of the sun or in man-made fusion reactors [3]. Cooler plasmas may be found in interstellar space or in flames. Within a plasma, the kinetic energy of electrons is often much higher than that of other species. This is because transfer of energy between heavy ions and lighter electrons is not efficient and thus leads to an unequal distribution of energy between the species. Where this is the case, the

plasma is referred to as non-thermal. Conversely, a thermal plasma is one in which all particles are in thermal equilibrium and is typically a characteristic of stellar matter [4].

Categorising a plasma as thermal or non-thermal is largely related to the frequency of collisions [4]. An increased number of collisions allows colliding species to reach thermal equilibrium more quickly. The frequency of collisions may be increased by increasing the pressure, and therefore pressure largely determines whether a plasma is thermal or non-thermal. However other factors may also have an effect on whether thermal equilibrium is reached. Should the dimension of the device be of a comparative length to the average distance between collisions, too few collisions will occur before species collide with the containing walls of the plasma, thus resulting in a non-thermal plasma. In effect, any factor affecting frequency or energy of collisions will determine whether the plasma is thermal or non-thermal. Pressure and dimension are two factors which will be examined in Section 1.4.2.

#### **1.1.4 Energy Distribution**

In a regular gas, the probability of a particle having a particular kinetic energy is described by the Maxwellian distribution function shown in Figure 1.1. This distribution describes the likelihood of occupation of different energy states. Non-thermal plasmas are described by a modified version of this distribution, which accounts for the higher proportion of high-energy electrons and thus features a longer tail in the high energy region [5].

This curve follows the Lorentzian distribution [6][7] and is shown in Figure 1.2. It is this distribution function which is expected of the plasmas examined and generated in this work. The high energy electrons in non-thermal plasmas give rise to different properties which become of interest when considering particular applications.

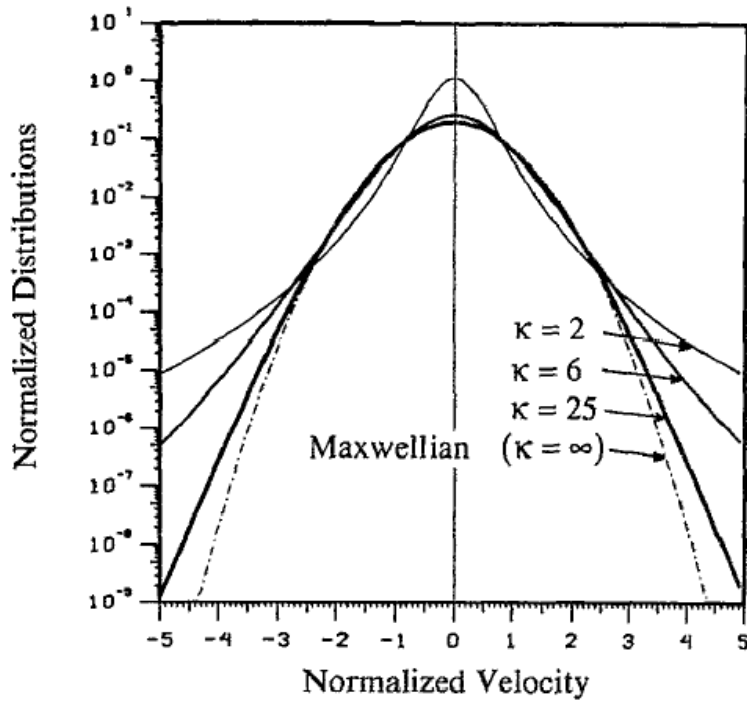


**Figure 1.1.** The normalised Maxwell-Boltzmann distribution curve ( $\kappa=\infty$ ) with corresponding Lorentzian distributions for different spectral indices [5].

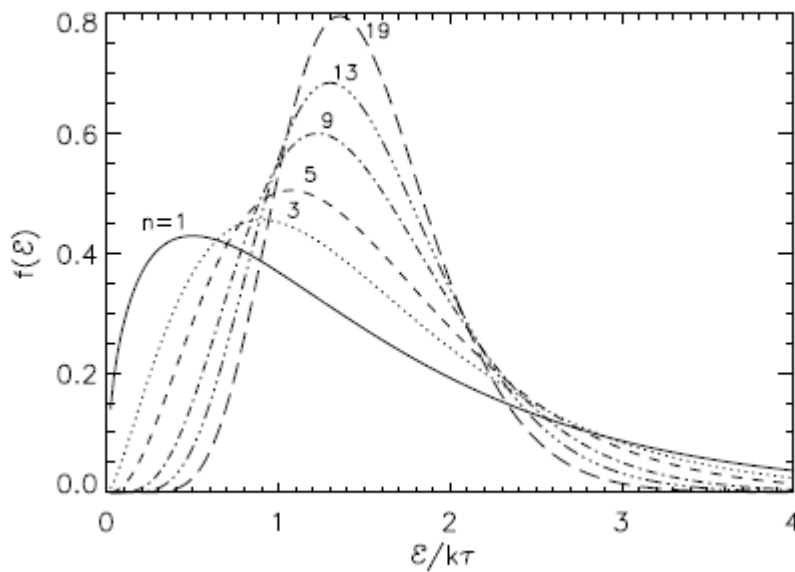


**Figure 1.2.** Non-thermal electron energy distribution function for different values of mean energy. The x-axis shows the energy of a free electron. The plot shows the characteristic high energy tail to the right of the peak. Taken from [8].

### 1.1.5 The Debye Length and Mean Free Path

The high proportion of charged particles existing in a plasma bring inter-charge forces to the fore of the plasma physics.

The force,  $F$  between two charges a distance  $r$  apart may be determined by the Coulomb law, as mathematically summarised in Equation (1).

$$F = k \frac{q_1 q_2}{r^2} \quad (1)$$

where  $q_1$  and  $q_2$  are two different charges and  $k$  is a constant.

The law describes how the force between two charged particles is proportional to the product of the magnitude of their charges, and inversely proportional to the square of the distance between them. Theoretically a particle at an infinite distance would feel the Coulombic effects from a point charge [2]. There exists in plasmas however a screening effect which prevents particles a certain distance away being affected by the Coulomb force [1][10][12].

Any one charged species in a plasma will be surrounded by a cloud of oppositely charged species. This has the effect of damping the Coulomb force felt by other particles in the plasma [9][10]. The distance over which this screening takes place is referred to as the Debye length after the Dutch physicist Peter Debye [11][13]. This screening effect reduces electrostatic potential energy between two oppositely charged particles from that given by the coulomb law (Equation (2)) to the screened potential (Equation (3)) where  $\lambda_D$  accounts for contributions from the Debye length for ions,  $\lambda_{Ds}$  (Equation (4)) and the Debye length for electrons,  $\lambda_{De}$  (Equation (5))[12].

$$U \propto \frac{q}{r} \quad (2)$$

$$U \propto \frac{q}{r} e^{-r/\lambda_D} \quad (3)$$

$$\lambda_{Ds}^2 = \frac{k_B T_s}{4\pi Z_s^2 n_s e^2} \quad (4)$$

$$\lambda_{De}^2 = \frac{k_B T_e}{4\pi n_e e^2} \quad (5)$$

It should be noted that these equations only hold for steady state, and were derived by considering the forces felt by a stationary charged particle introduced to the plasma. The plasma is also assumed to be in thermal equilibrium, for which the ion Debye length is much greater than that of electrons.

In order for a plasma to remain in a stable state, the Debye length must be smaller than the dimensions of the plasma [13]. If this was not the case, all charged species within the plasma would feel the Coulomb force and so would be attracted towards each other and would recombine into atoms.

The Debye length plays an important role in understanding the frequency of collisions within a plasma, and how this differs from other states of matter. The probability of a collision occurring between any randomly moving particles depends on the velocity of the particles, the density of the particles and the sphere of influence of the particles. For neutral particles, the sphere of influence is simply their physical volume. However, for particles in plasmas which are charged, the sphere of influence is the sphere within which the Coulomb force may be felt by another particle, i.e. the Debye length [2][13][19].

A smaller sphere of influence results in particles travelling further between each collision and therefore collisions are less frequent. In a gas the sphere of influence is smaller than that in a plasma and so the average distance travelled between collisions by gas particles is larger than that in a plasma. This average distance between collisions is referred to as the mean free path of the particles and is smaller for a plasma than a gas of the same density [13].

In a plasma, the mean free path of particles increases upon increasing velocity. This is because particles with a high kinetic energy may travel closer to similarly charged particles before being repelled, as they require a stronger repulsion force to change their direction. The Debye Length of an ion is therefore reduced in magnitude and so the mean free path increases. This gives an inversely proportional relationship between particle velocity and mean free path. In a gas however, the sphere of influence is simply the volume of the particle and so is not affected by velocity [1][2][10][13].

Collision frequency between particles in any state is inversely proportional to mean free path. In a plasma, increasing the speed of particles increases their mean free path, therefore decreasing the frequency of collisions. This is contrary to collision frequency observed in a gas, where increasing the kinetic energy of particles increases the frequency of collisions [13]. Therefore, upon increasing the temperature of a plasma, the collision frequency decreases. Increasing the pressure however decreases the mean free path, therefore giving a higher collision frequency. This results in a higher number of ionising collisions and a higher average density of the plasma [19].

### **1.1.6 Existence of Plasmas**

The majority of plasma matter in the universe exists in interstellar space and in stars. These plasmas are examples of high temperature plasmas, at temperatures of over  $10^7$  K [2] and are similar to the artificially created plasmas in fusion reactors. Due to the relatively low temperatures and high pressures of the Earth's atmosphere, terrestrial plasmas are less commonly occurring than in the majority of the universe [81]. However under certain conditions plasmas may exist on Earth, both naturally and artificially. Lightning and the aurora are both examples of naturally occurring plasmas within the Earth's atmosphere [13].

The properties of artificial plasmas vary depending upon the conditions in which they are created and contained. Variable parameters such as temperature, pressure, power source, electrode configuration and magnetic field presence determine the characteristics of a plasma.

The focus of this review will be on a variety of artificial plasmas known as gas discharges.

## 1.2 Gas Discharge Plasmas and the Hollow Cathode Discharge

### 1.2.1 Gas Discharge Plasmas

There are several methods by which a plasma may be created, all of which involve removing electrons from their atoms in order to create positive ions and electrons. One of the simplest methods of achieving this is to pass a high voltage between electrodes in the presence of a gas. A sufficiently high potential difference across electrodes, known as the break-down voltage, causes the gas to dissociate into electrons and positive ions. The process by which this occurs is outlined below.

Electrons emitted from the cathode are accelerated towards the anode and collide with gas molecules as shown in Figure 1.3. Inelastic collisions are the most important in the case of the gas discharge and may be either excitation or ionisation collisions [4]. The latter produces one or more newly ionised electrons which will be accelerated in the electric field and proceed to collide with further atoms [14][15]. In a stable state, charge neutrality of the plasma is conserved as an approximately equal number of positive and negatively charged particles are produced in each collision. Excitation collisions simply promote atomic electrons to a higher energy level [16]. Relaxation from this level leads to photon emission, producing the glow which is characteristic of discharge plasmas [17][18]. Plasmas produced in this way use direct current although other types of current may be used [47]. The gas used may be varied depending on the application required, several of which are discussed in Section 1.5.7.

Besides the discharge itself, collisions also occur at the surfaces containing the plasma. Upon collision with a surface, particles, be they photons, ions, electrons or neutrals, may eject an electron from a surface, assuming they have sufficient energy to do so [19]. This bombardment process, known as sputtering, produces secondary electrons, further contributing to the electron density within the gas discharge and increasing the negative charge at the surfaces [20][21]. A property of the material known as the work function determines how much energy is required to release an electron from its surface [22]. This factor therefore is one of potential importance when considering a material from which to fabricate a gas discharge. Collision with the container surfaces also results in a heating effect and a loss of energy from the plasma [23].

Upon reaching the anode or upon collision with a surface, electrons may also recombine with ions or add to neutrals to produce negative ions, and thus the charge composition of the plasma is changed [24]. In order for the net charge to remain constant, or close to zero, there must be sufficient ionisation collisions in the plasma to sustain the ratio between positive and negatively charged species. Therefore, for the plasma conditions to be maintained, electrons must acquire sufficient kinetic energy from the applied field to ionise atoms upon collision [25]. This implies that there is a lower limit to the potential difference which may be applied across the electrodes for a discharge to be sustained [26]. This potential varies and is described by the Paschen law [27] in Section 1.4.1.

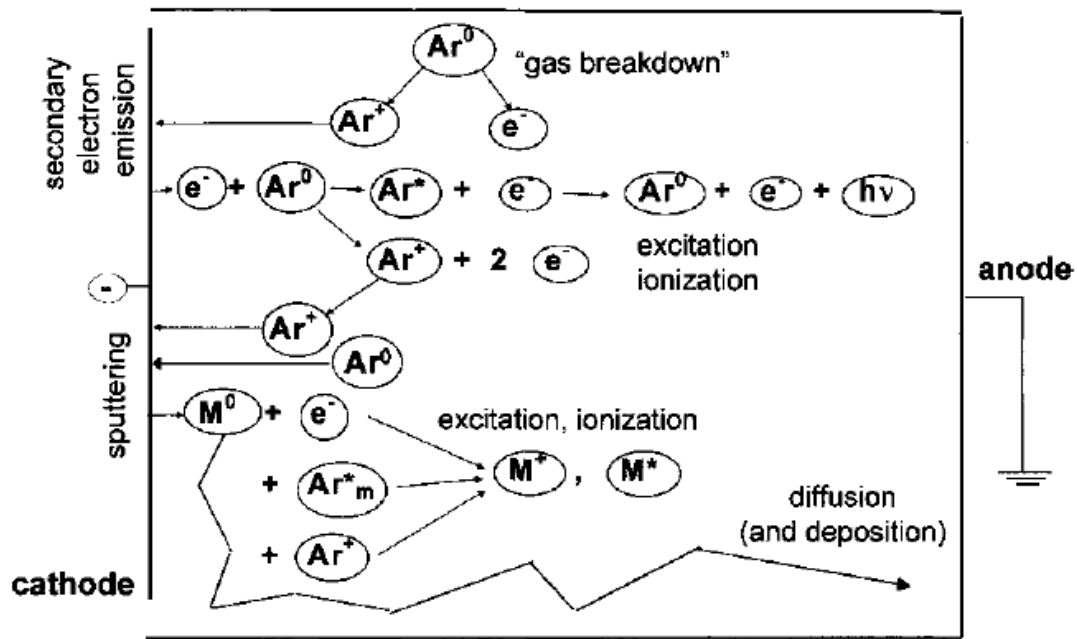


**Figure 1.3.** An example of a simple glow discharge tube in an argon atmosphere and the collisions occurring within. The cascade process may be seen in which a single electron produces further electrons and ions on collision. The sputtering process may also be seen, leading to degradation of the electrodes shown by the metal ion  $M^0$ . [4].

### 1.2.2 Regions of a gas discharge

In contained plasmas, such as a gas discharge, a Debye shielding effect may be seen at the walls similar to the effect mentioned in Section 1.1.5. The high electron density at the walls due to secondary emission results in an electron repulsion in the region of space directly adjacent to the wall and therefore proportionally a higher concentration of positively charged species [28]. As electron collisions are responsible for photoemission, this region is darker than the main body of the discharge and is often referred to as the dark region or sheath [29].

The collision and discharge processes in glow discharges are complex and much experimentation and modelling has been carried out in order to produce accurate models [30]. Figure 1.4 shows a cross section of a gas discharge tube and the variation between regions within it.

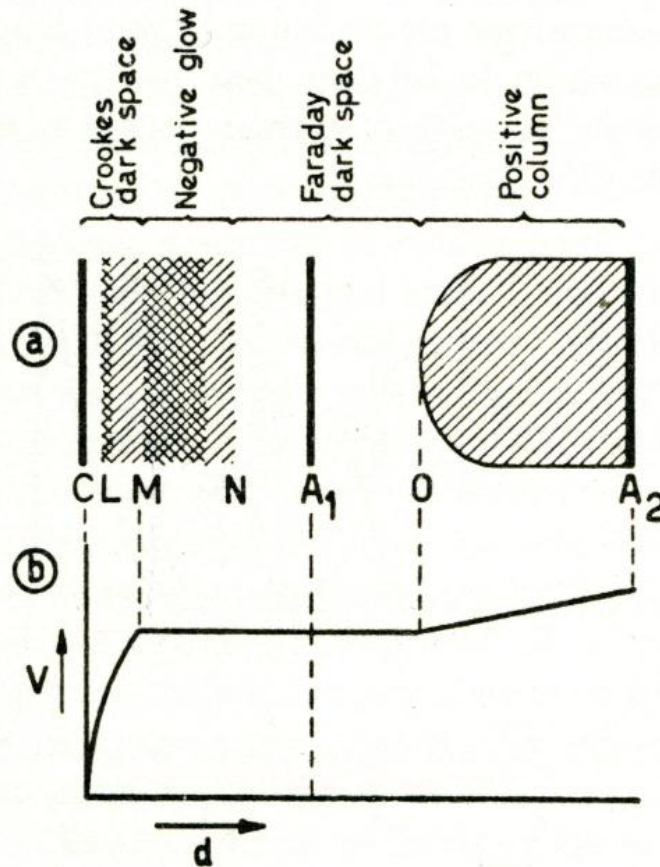


**Figure 1.4.** (a) Schematic diagram showing regions within a glow discharge tube. (b) shows how the voltage changes with distance from the cathode. Taken from [42].

The main source of light comes from the excitation collisions within the positive column. The region between C and M (cathode fall region) is the distance across which the majority of potential drop occurs, as can be seen from the voltage plot [31]. The region between M and N (negative glow) is a second region of glow discharge, occurring as a result of increased charge density at the anode end of the cathode dark space. This charge density creates a slightly negative potential, reducing further acceleration. Electron energy is absorbed upon ionisation and excitation, causing the characteristic bright glow of the negative glow region [32].

The nature of the discharge between the electrodes depends on the voltage and current applied. At electrical powers higher than that required for breakdown, the discharge takes on different forms [31][32][42].

Figure 1.5 provides a schematic representation of these forms, illustrating the discharge dependence on current and voltage parameters. The section in

Figure 1.5 between E and F is the region for which the glow discharge is self-sustaining and abnormal. When the current increases past the current at F, the glow enters the arc discharge mode and becomes unstable.

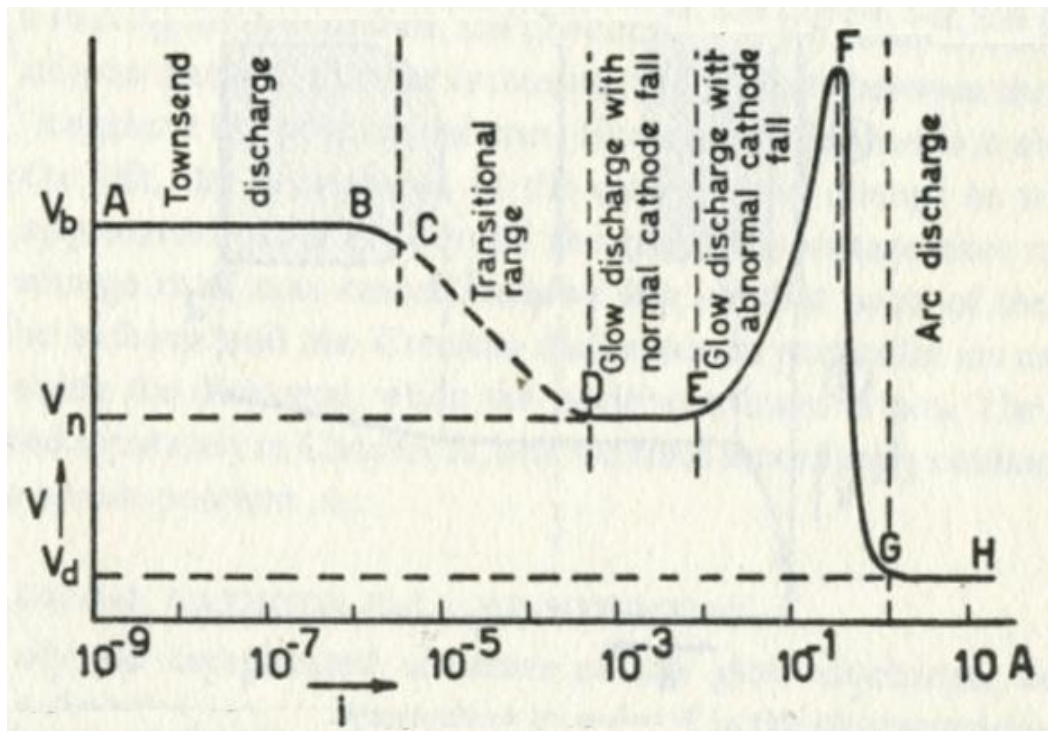


**Figure 1.5** Current-voltage characteristic for a glow discharge column, showing different modes of operation.  
 Taken from [42].

## 1.3 The Hollow Cathode Discharge

### 1.3.1 Introduction to the Hollow Cathode Discharge

Operation of a gas discharge using parallel electrodes is not always stable and favours lower pressure operation a few Torr [14]. Above certain pressures, ions and electrons may escape through the gap between the electrodes. A simple schematic diagram of this arrangement is shown in Figure 1.6.

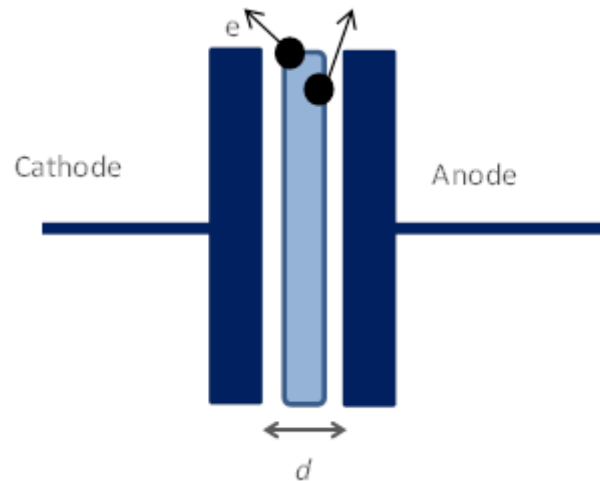


**Figure 1.6.** Schematic diagram of a parallel plate electrical discharge arrangement. Electrons have been added to demonstrate the lack of enclosure.

An improvement on this arrangement is the hollow cathode geometry Figure 1.7 [33]. Used for over 100 years, the geometry allows a stable discharge to form inside the cathode's cavity [34] [35]. Compared with the parallel plate geometry, the hollow cathode has fewer pathways from which electrons and ions may escape, raising its stability and thus supporting high electron densities [36] [55] [67]. Of the possible geometries for the hollow cathode discharge (Figure 1.7), a simple sandwich structure (Figure 1.7 (c)) is favoured simply for ease of fabrication [66]. As the anode does not have a great impact on the physics of the discharge [37], this is often the geometry used to create a hollow cathode discharge.

Depending on the pressure and discharge current, the glow discharge will form almost entirely within the cavity [38]. A discharge formed in this arrangement features different properties from planar and tube glow discharges and does not feature all of the regions as described in Section 1.2.2.

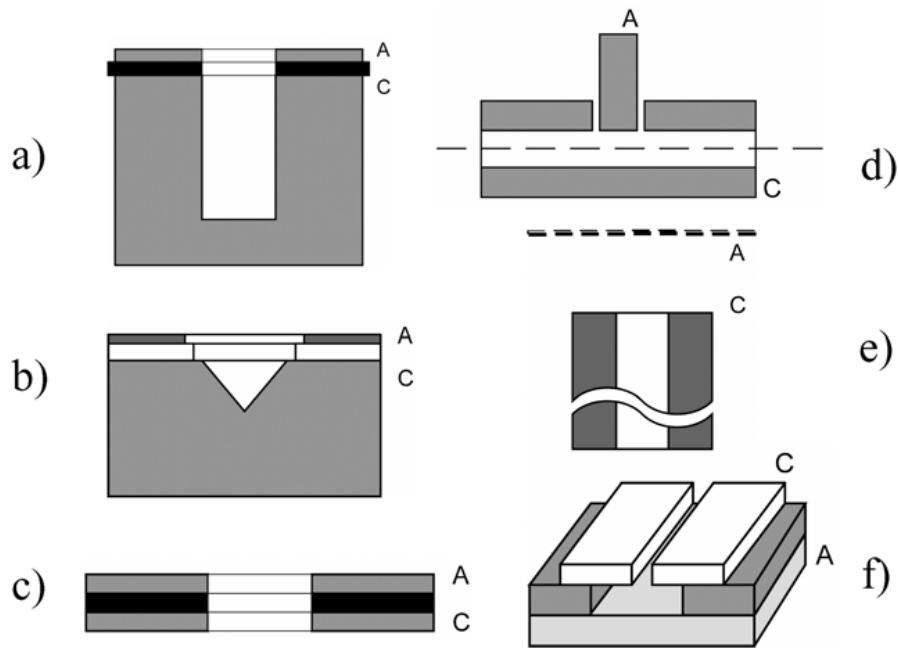


**Figure 1.7.** Possible geometries of a hollow-cathode discharge. Anode labelled as A; cathode labelled as C. Taken from [66].

### 1.3.2 Modes of the Hollow Cathode Discharge

As for all gas discharges, both current and pressure affect the optical and resistive properties of the discharge. Shown in

Figure 1.8 is a schematic diagram of voltage against current, showing the characteristic modes of the glow discharge. The hollow cathode discharge mode is characterised by a cylindrical symmetry about the cathode hole and a negative differential resistivity [67]. When the current is increased above the Townsend discharge mode, a virtual anode is formed from the discharge column inside the cavity due to an increase in electrical conductivity [57]. In the Townsend discharge region, the electric field is axial. This then changes to a more radial field to compensate for electron losses in the virtual anode. The strong radial field causes electrons to oscillate about the central cavity axis [39] leading to an increased number of ionising collisions as electrons gain higher energy in the radial field. This leads to an increase in current and a decrease in voltage needed to sustain the discharge. This can be seen in

Figure 1.8 as the negative resistivity section in the hollow cathode discharge mode. Further increasing the current leads to the abnormal glow mode, in which instabilities are more likely to occur [71].

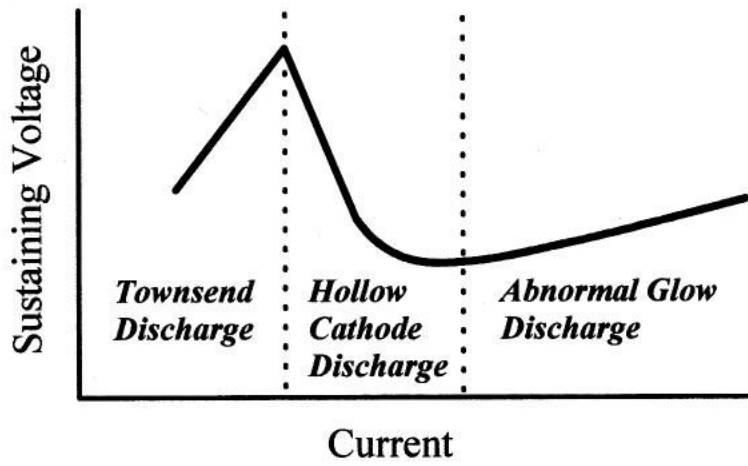


**Figure 1.8.** The voltage-current characteristic of a microhollow cathode discharge. The current scale is logarithmic. Taken from [57].

## 1.4 High Pressure Discharges

Glow discharge tubes and hollow cathode discharge devices (as described above) are commonly operated below atmospheric pressure [14][66]. However, it is possible to sustain hollow cathode discharges at atmospheric pressure [39][40][66] and this possibility greatly widens the range of applications such plasmas may be used for. Under high pressures however, certain instabilities come to light and several parameters must be considered in order to maintain the discharge (Sections 1.4.1, 1.4.2). Once struck, the energy of species involved in collisions must be higher than the ionisation energy of the gas, so that the discharge is sustained. As a result, they do not readily form at extreme high or low pressures.

### 1.4.1 Paschen Law and Breakdown Voltage

In order for a discharge to be sustained, electrons ionised and released at the cathode must ionise further electrons before reaching the anode. This implies that their mean free path of ionisation must be smaller than the cathode-anode separation. As the mean free path decreases with increasing pressure, the cathode-anode separation must be reduced in order to maintain this relationship. The limiting values of  $p$  and  $d$  may therefore be characterised by the product  $pd$  and is derived from the Paschen scaling law [41][66].

The breakdown voltage  $V_b$  is determined by the product  $pd$  where  $p$  is the pressure and  $d$  the distance between electrodes. This is a result of Paschen's law which describes  $V_b$  as a function of the product of  $p$  and  $d$  [42]. Plotting  $V_b$  against  $pd$  gives a distinctive curve, characteristic of any combination of electrode material and gas. The curve gives a breakdown voltage which is unique to the gas, electrode separation and pressure (Figure 1.9). Reducing the electrode separation allows higher pressure operation of the discharge. By altering the electrode scale to the order of microns, direct current plasmas may be sustained above atmospheric pressure [46].

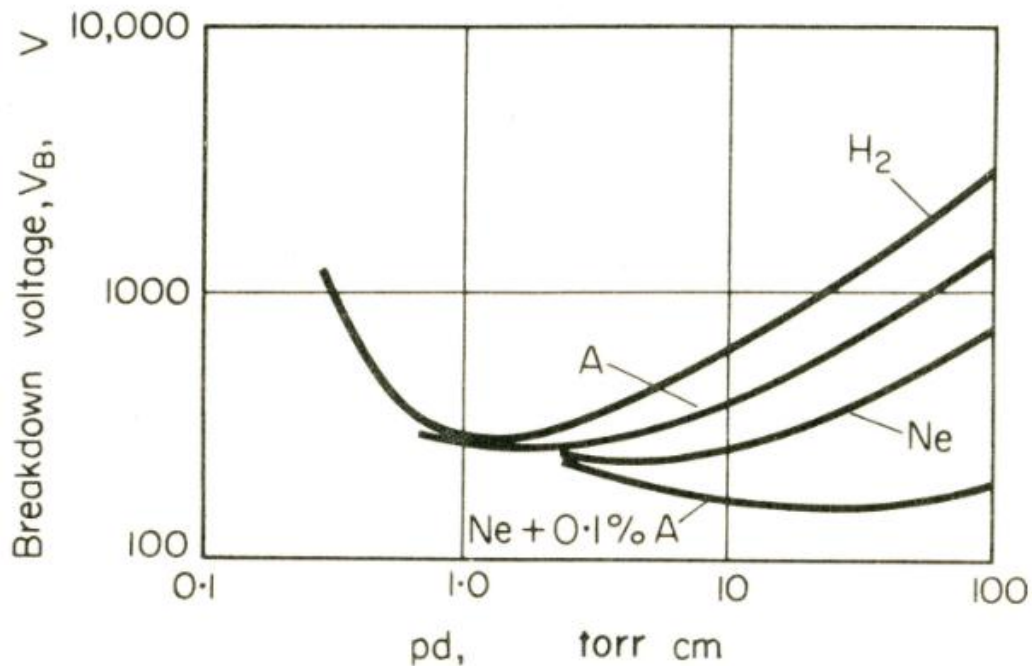


**Figure 1.9.** Paschen curves for discharges in argon (A), neon (Ne), hydrogen ( $H_2$ ) and a Ne-Ar gas mixture. The minimum breakdown voltage occurs for a unique value of  $pd$  dependant on the gas used [32].

The breakdown voltage,  $V_b$  is commonly in the range of 0.1 to 10 Torr cm [43]. The minimum may be explained by considering theory of collisions. On increasing pressure, more collisions occur. However the energy gained on each collision is lower and therefore a higher voltage is needed for a collision to cause ionisation. This gives rise to the almost linear relationship to the right of the minimum. To the left of the minimum, collisions are much less frequent, therefore requiring a higher voltage to maintain the ionisation. High pressures and small scales may cause deviations from the typical Paschen curve as examined in Section 1.5.4.

#### 1.4.2 The $pD$ Scaling Law

A second scaling factor unique to the hollow cathode discharge is the product  $pD$ . It has been found experimentally that the discharge voltage remains constant if the product of  $pD$  is constant as described by the Allis-White similarity law [38]. This results from the condition that the negative glow region (see Section 0) from opposite sides of the cathode must interact for a hollow cathode effect to occur. There will be overlap between opposite and adjacent sides of the cathode if the cathode diameter multiplied by pressure is of the order of 10 Torr cm [44]. The limit of this product has been determined to be between 0.026 Torr cm and around 10 Torr cm although these limits are affected slightly by the ionising gas used [45].

This range has also been clarified by Schoenbach [65] and further experimentation into the characteristics of the hollow cathode discharge for  $pD$  values in the range of 0.1 Torr cm to 10 Torr cm have been examined. Successful operation of a hollow cathode discharge has been carried out at  $pD$  values of up to 5 Torr cm in argon corresponding to a pressure of 250 Torr and a 200  $\mu$ m cathode

hole [73]. A hollow cathode discharge has been sustained in atmospheric pressure by reducing the hole diameter to the order of 100  $\mu\text{m}$  [46]. The lower limit of the product  $pD$  is given by the same condition as the product  $pd$ , namely that the mean free path of ionisation must not exceed the dimensions of the apparatus [83]. The upper limit of the product  $pD$  has not been as clearly defined, although experiments have been carried out with the aim of investigating the  $pD$  range. It was found by Schoenbach [65] that changing the  $pD$  value had an effect on the appearance and optical properties of the discharge.

## 1.5 Microplasmas

### 1.5.1 Introduction to Microplasmas

Microplasmas are electrical discharges in which one of the dimensions is 1 mm or less and often take the form a scaled-down version of the hollow-cathode geometry (see Figure 1.7) [66].

As with the hollow cathode discharge, they may exist in several geometries. The geometry focused on in this work is that of the cylindrical cavity, a simplified cross-sectional version of which is shown in Figure 1.10.

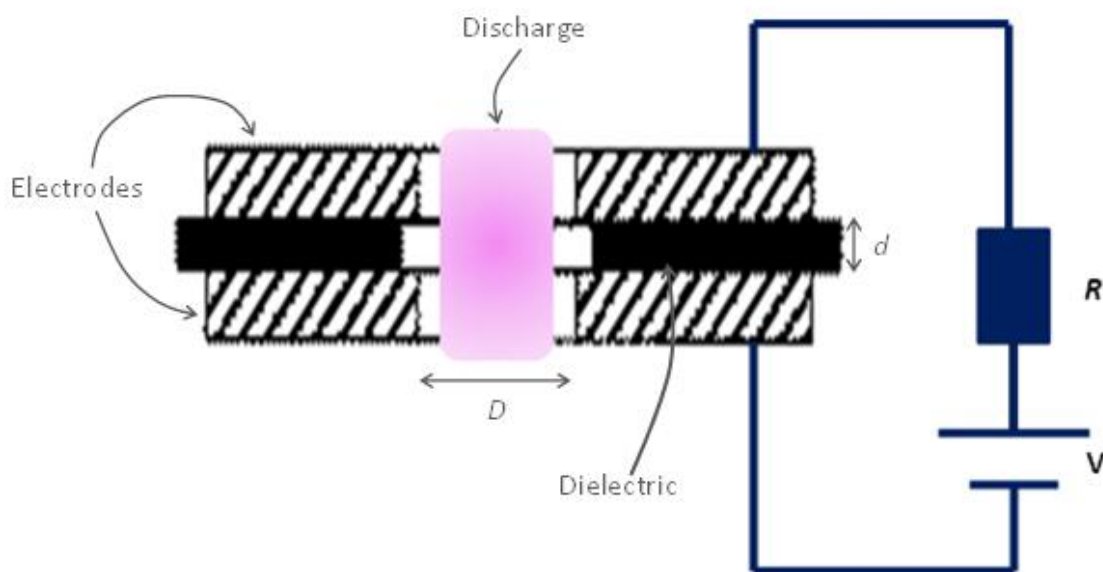


**Figure 1.10.** Schematic diagram showing the cross section of a microplasma device with a cylindrical cavity. The simple circuit demonstrates the application of a potential difference between the two electrodes. *Note: this diagram is not to scale.*

By reducing the dimensions  $d$  and  $D$  of this device, direct current plasmas may be sustained above atmospheric pressure [46] as a result of the scaling laws  $pd$  and  $pD$  (Sections 1.4.1, 1.4.2). Due to their small dimensions, surface effects such as cathode heating and wall losses (see Section 1.5.2) become increasingly prominent. The material used to contain the discharge must therefore be carefully chosen to match the characteristics of the device (Section 1.5.6). Operation at high pressure (atmospheric and above) brings to light several instabilities (Section 1.5.3) which must be minimised for the devices to become suitable for a range of applications (Section 1.5.7) and become commercially viable.

## 1.5.2 Ion and Electron Kinetics in Microplasma Devices

Much computational and mathematical modelling has been carried out in order to determine the properties of the discharge inside microplasma devices [47][48] and how they differ from larger scale, low pressure devices. At atmospheric pressure, the energy of ions colliding with the cathode is much lower than that in a low-pressure device. This is because most ions lose their energy through collisions within the bulk of the plasma, and incur many collisions as their mean free path is much smaller than the sheath width. Upon increases in pressure, the mean free path is reduced, resulting in a higher frequency of collisions. In general this results in species rapidly losing energy within the bulk of the plasma [49][50][51].

It is known [52][71] that the cathode fall region is one of high electric field. The higher electric fields present in micron-scale devices causes a higher acceleration of secondary electrons (Section 1.2.1) across the cathode fall region [47]. As a result, most ionisation occurs near the cathode and its temperature is much higher than the bulk of the discharge. This region is the primary source of instabilities when high pressures are reached [53][47][54].

High electron densities characteristic of small scale discharges cause significant erosion of electrodes and surfaces of the containing vessel through sputtering [55][56]. Measurement of power throughout the discharge shows that the highest proportion of power is lost near the cathode (Figure 1.11). Dissipation of high gas temperatures away from the surfaces in contact with the plasma may therefore increase the stability and lifetime of these discharges.

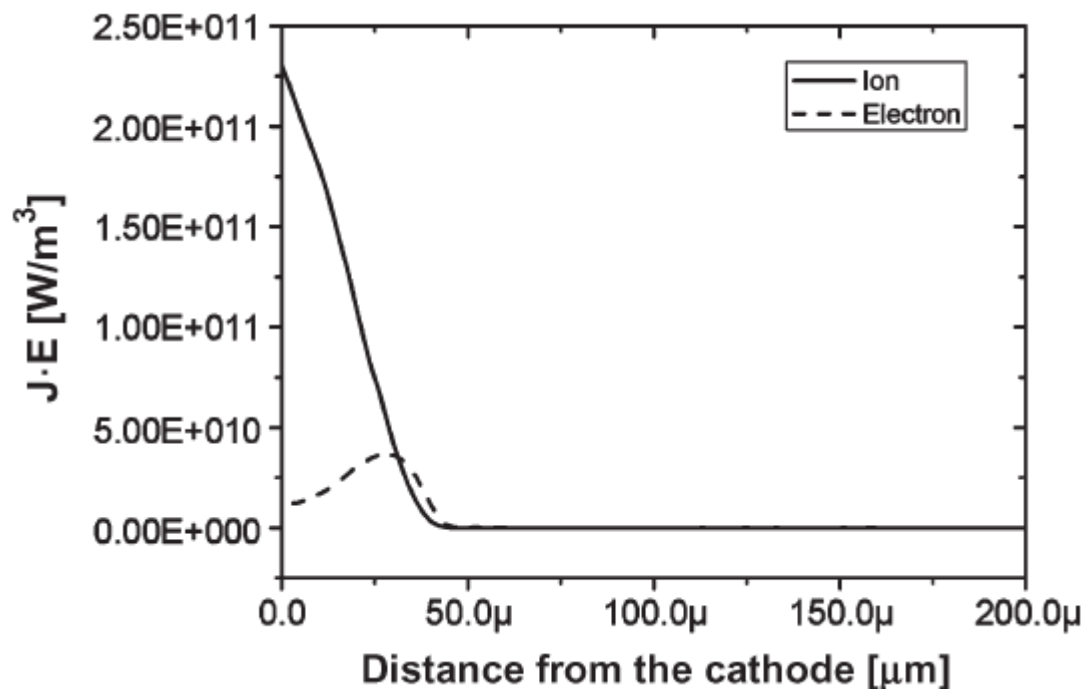


**Figure 1.11.** Power absorption as a function of distance from the cathode in a DC helium microplasma at atmospheric pressure [47].

### 1.5.3 Instabilities

The majority of significant instabilities occur in regions near electrodes, primarily in the cathode region. The cathode region is the region of highest electric field and therefore higher power density compared to the positive column [71]. This is the region where instabilities are most likely to arise and which determine the restrictions on the parameters of operation. The charge density in the bulk of the discharge increases linearly with pressure, whereas in the cathode region it increases quadratically with pressure [29][57]. In general, current density increases with pressure, implying a maximum pressure at which the glow discharge will operate without instabilities occurring.

Arcing (glow-to-arc transition) occurs in non-thermal plasmas, generally when a current or pressure threshold is surpassed [29][58]. The glow-to-arc transition is the conduction of electrons via a direct channel, short-circuiting the glow-discharge, and therefore leading to its breakdown. It is the primary source of instability in high pressure glow discharges [52]. Due to the high field near the cathode, electrons are drawn from the cathode, ionising further atoms and creating positively charged ions. These positive ions further increase the electric field strength, leading to extraction of more electrons. This can result in an unstable cycle producing a current which bypasses the glow discharge [29][53].

Due to the reduced scale of microplasmas, the characteristics of the discharge change and become dependent on the cavity geometry. It is thought that sheath region inside the cavity becomes small to the point of disappearing [94]. For the sheaths to exist at such high pressure would require electron densities of greater than  $10^{14} \text{ cm}^{-3}$  [59]. The mode of discharge is no longer that of a hollow cathode but is in the form of a negative glow. Later modelling work [59] characterised the dependence of sheath width on pressure to be inversely proportional and also modelled the discharge as a negative glow. As may be seen in Figure 1.12 the sheath thickness may become negligible at higher than atmospheric pressure and in microplasmas of such small dimensions.

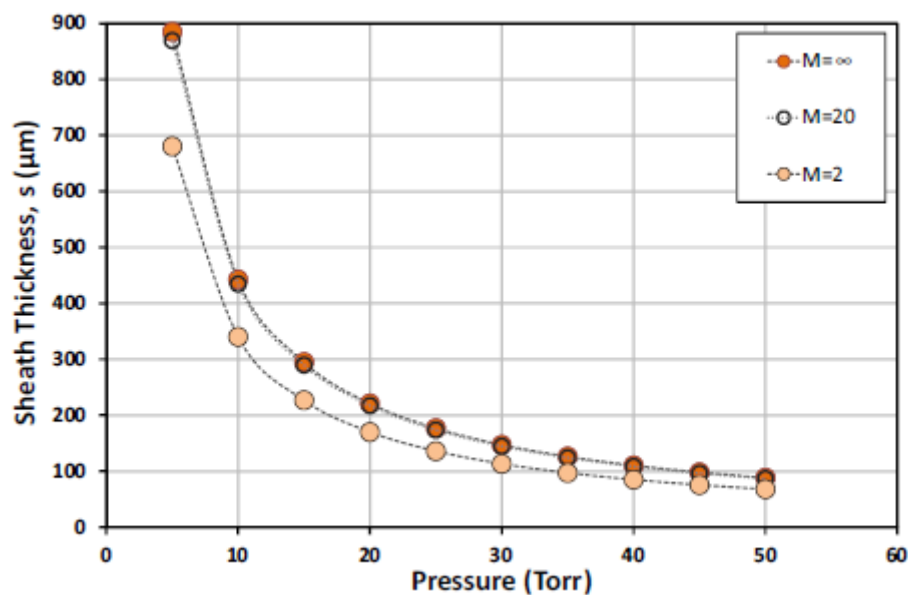


**Figure 1.12.** Plot to show how sheath thickness varies with pressure. M is the ion multiplication factor describing the strength of ionisation within the sheath [59][60].

### 1.5.4 The Breakdown of the Paschen Curve

The increasing work with micron scale electrical discharges has brought to light deviations from the aforementioned (Section 1.4.1) Paschen scaling law [60]. The Paschen curve predicts that on increasing  $pd$ , the breakdown voltage will also decrease until a minimum is reached, beyond which further increases in  $pd$  result in a rise in  $V_b$ . The presence of the minimum is due to the rapid loss of electrons to the surfaces which occurs when the electrode gap is small. However, experimental work [61] has found that for small scale discharges,  $V_b$  continues to decrease with  $pd$ , below the minimum predicted. Figure 1.13 shows a mathematical model produced for the Paschen curve which takes into account the effects that occur when using small cavities.

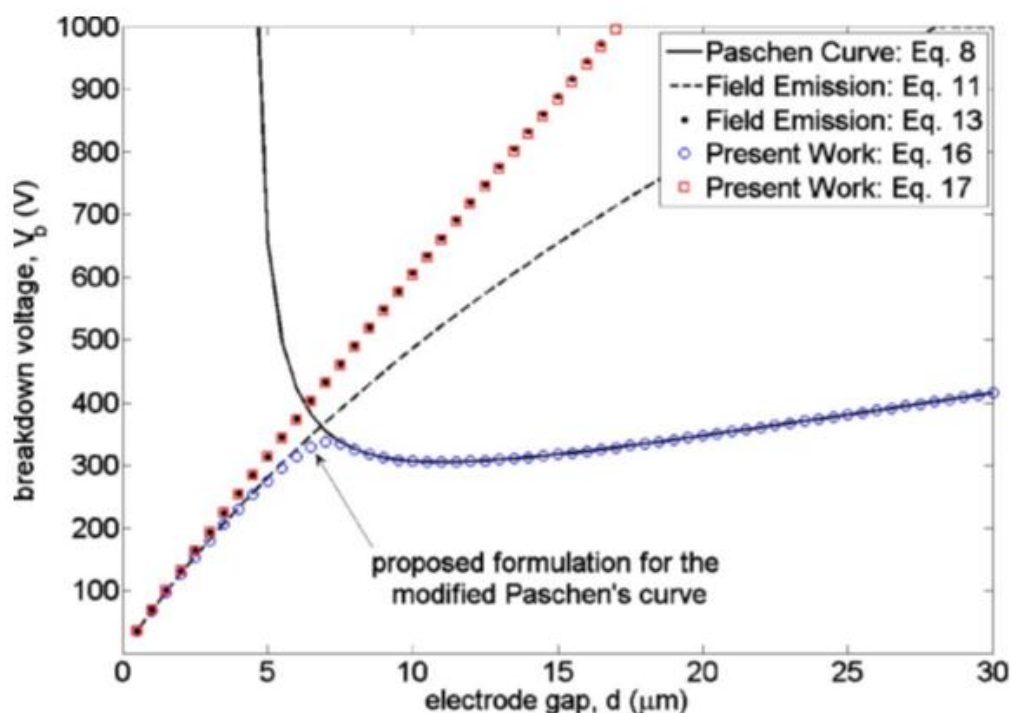


**Figure 1.13.** The revised model of the Paschen curve for small scale discharges. The two lines of concern are the Paschen curve (solid black) and the proposed new model for the Paschen curve (blue circles). Plot taken from [62].

The proposed theory is based on increased electron field emission due to the high electric field between the electrode gap of micro-scale dimensions. The high electric field draws electrons away from the surfaces, compensating for the electron losses which contribute to the necessary increase in  $V_b$ . This high electric field occurring in micron gaps therefore has the overall effect of lowering the voltage required to cause electrical breakdown, upon reaching geometries of around 10 microns and below [61][62][63].

### 1.5.5 Optical properties and modes of discharges

Reducing the geometry of hollow cathode discharges has an impact on the intensity and range of emission produced and hence the spectroscopic characteristics are affected. The radiation from microdischarges with dimensions less than 200  $\mu\text{m}$  covers a broad spectral range [46].

The optical and spectroscopic properties of hollow cathode discharges are dependent on the product  $pD$ . The glow discharge appearance also depends upon the operational current [64]. For a typical hollow cathode discharge mode, the discharge is symmetrical about the cathode hole, forming a circular ring at low currents, and becoming a more closed ring with increasing current [38]. The  $I$ - $V$  curve features a negative gradient during the hollow cathode discharge mode [57][65]. Using these distinctive characteristics, it is possible to investigate the effect of changing the product  $pD$  on the appearance of the discharge.

Shown in Figure 1.14 is the effect of increasing the dc current on the appearance of a discharge operated at a  $pD$  value of around 5 Torr cm taken from work by Schoenbach [65]. The ring formation may be observed, which disappears with the negative  $I$ - $V$  curve, and this is similar for a  $pD$  value of 1.1 Torr cm. In comparison to the discharges shown in Figure 1.14, shown in Figure 1.15 is the discharge appearance for a  $pD$  value of 17.9 Torr cm. With increased pressure, the discharge becomes much larger and the ring less defined. The distinctive negative resistivity no longer appears and the  $I$ - $V$  curve does not follow the similar properties of lower pressures. This suggests that discharges with a  $pD$  higher than 5 Torr cm may not have characteristics of the hollow cathode mode of operation, although they may still be stable discharges.

Figure 1.16 shows the negative resistivity characteristic, distinctive of high pressure discharges in the hollow cathode mode. The deviation at around 2 mA is due to the transferal of the glow discharge from the face of the cathode to the cavity.

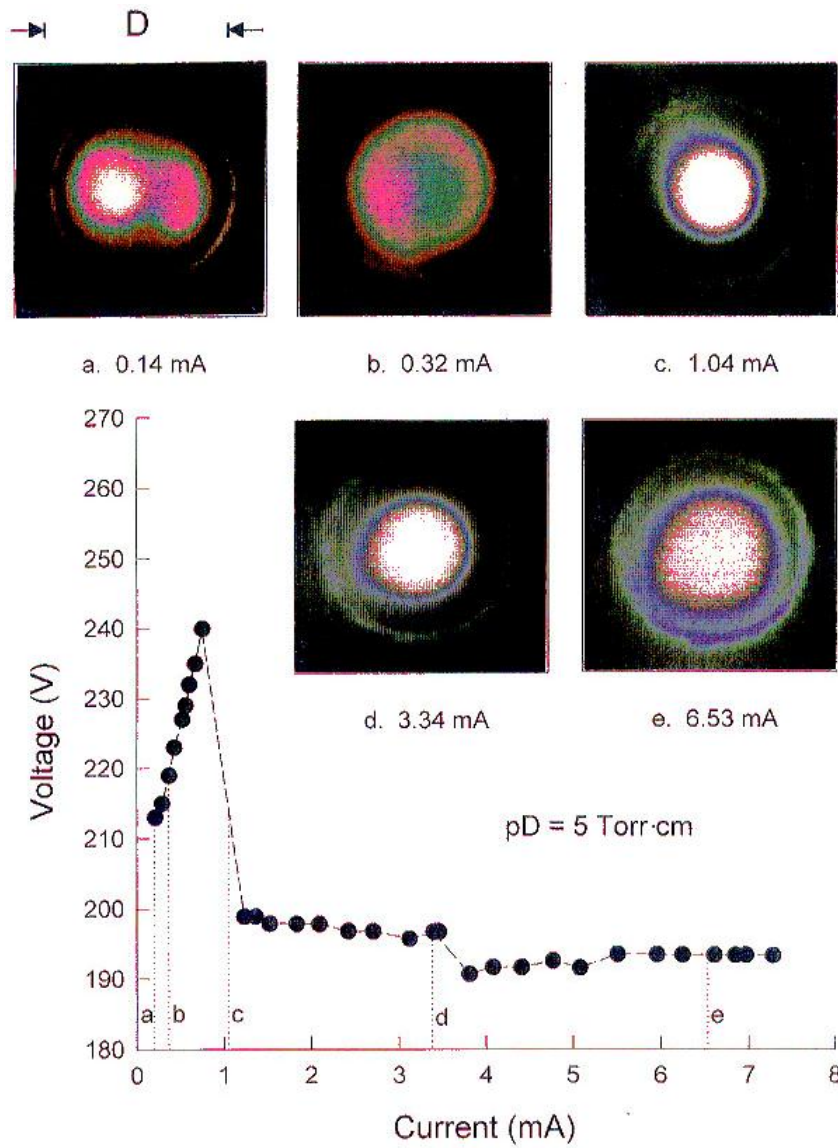


**Figure 1.14.** End-on photographs of the discharge produced by a hollow cathode discharge. The gas was argon at a pressure of 250 Torr and a cathode diameter of 200  $\mu\text{m}$ . Taken from work by Schoenbach et al [65].

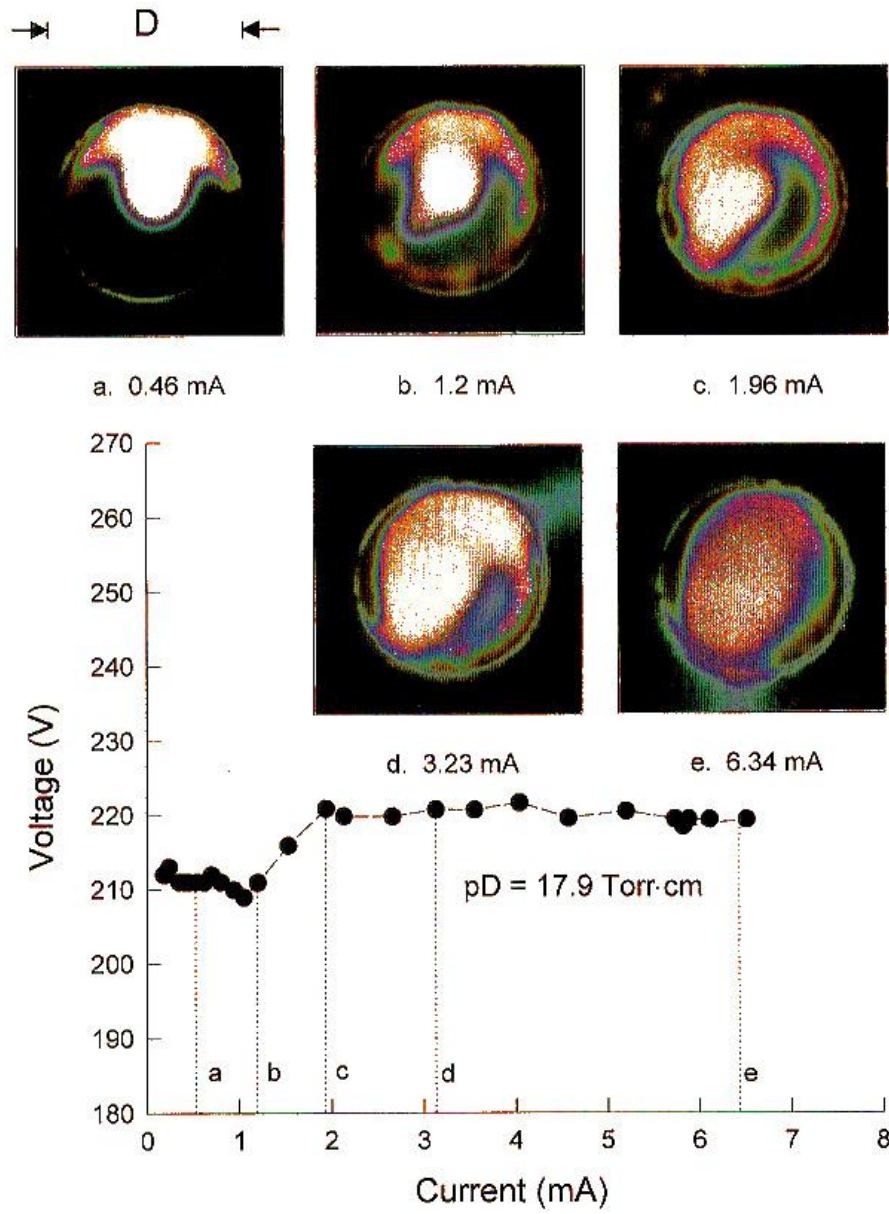


**Figure 1.15.** End-on photographs of the discharge produced by a hollow cathode discharge geometry. The gas was argon at a pressure of 896 Torr and a cathode diameter of 200  $\mu\text{m}$ . Taken from [65].

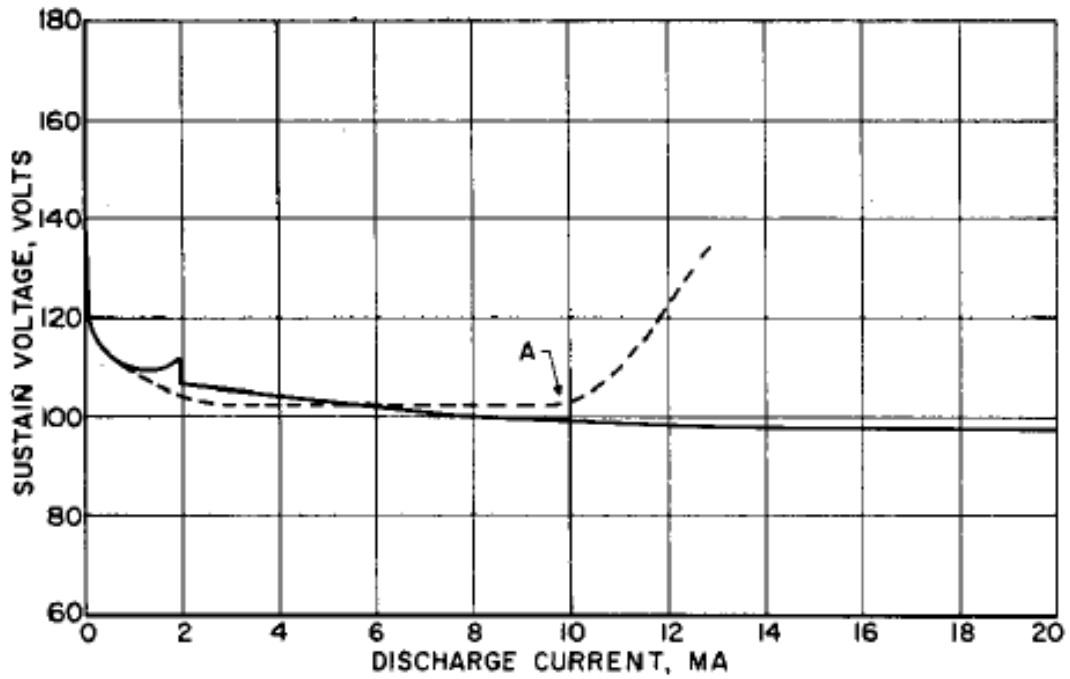


**Figure 1.16.** Current-voltage characteristic of a  $0.075 \mu\text{m}$  hollow cathode discharge represented by the solid line, and that of a plane cathode discharge with 20 times the area (dashed line) both under a neon gas at 100 Torr (0.131 atm). Taken from [44].

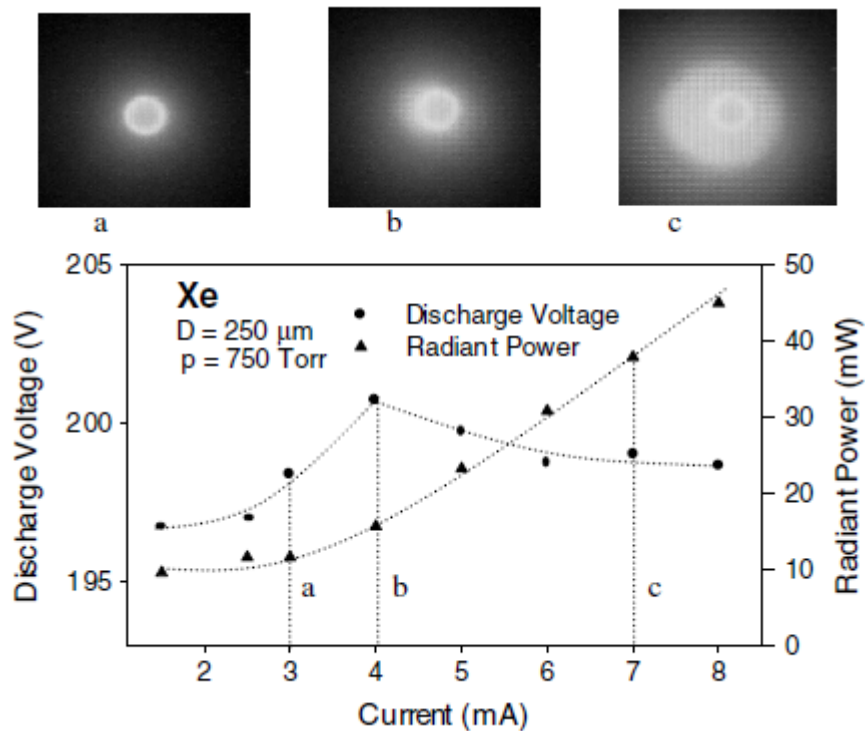


**Figure 1.17.** Current-voltage curve together with the optical properties of the discharge for different modes of operation. Taken from [66].

It has been observed that the hollow cathode discharge mode ceases for  $pd$  of greater than around 4 Torr cm. The discharge instead resembles an abnormal glow. Figure 1.17 shows how the I-V plot behaves above the negative glow discharge conditions.

The transition from positive to negative differential resistance is attributed to the transition from the abnormal glow inside the cavity to a normal glow covering the outer cathode surface. If the glow spreads to cover part of the surface, the discharge may again be in the abnormal mode [67].

### 1.5.6 Materials and Fabrication

In micron scale discharges, the surfaces of the containing vessel become increasingly important due to the plasma's high surface-area-to-volume ratio. The material used for the device therefore must be chosen carefully and several materials have been studied [4][66][81].

Common to all arrangements of the microplasma is the presence of two electrodes, a cavity, and an insulating dielectric. The entire device must be resistant to chemically reactive ionised species within the discharge and have a high thermal conductivity in order to dissipate heating effects. In addition, the insulating dielectric must have a high resistivity whereas the electrodes must have a high conductivity.

For the electrodes, molybdenum is often favoured for high current operation (greater than 1mA) due to its higher melting point [68][69]. Other metals such as nickel, silver, copper and platinum have been found to be suitable electrodes for slightly lower current operation [70][71][72]. Despite its lower melting temperature, gold has also been used as an electrode [73] due to its high conductivity.

The use of silicon enables complex geometries to be fabricated using reaction ion etching techniques to create the desired geometries [74][75].

The insulating dielectric is of great importance and will shape the electric field formed within the cavity [74]. Constant bombardment by high energy electrons means the dielectric and its properties will influence the electron density within the discharge [71]. Alumina, boron nitride and molybdenum have been used for high temperature operation, such as that in air [76][77] whilst mica, polymers and SiO<sub>2</sub> have also been used. In order to become commercially viable, the device must be capable of running for long time periods without destruction. The properties of diamond, (Section 1.6) make it a promising material for an entire microplasma device, in both its doped and un-doped forms.

As well as device materials, a variety of background gases have been experimented with. The main impact of the operating gas is on the breakdown voltage (see Section 1.4.1) and optical characteristics. The noble gases are the most common for use in microplasmas and produce the normal and abnormal modes of operation [55] however combination gases may be used and devices have successfully been operated in atmospheric air [76][77]. The thermal conductivity of the gas used has some impact on the nature of the plasma, although is primarily of importance when considering thermal plasmas [78]. A greater degree of ionisation will lead to a higher thermal conductivity, thus a more even temperature distribution throughout the plasma. Helium has a

relatively high thermal conductivity ( $0.142 \text{ W m}^{-1}\text{K}^{-1}$ ), in comparison to other noble gases such as argon ( $0.016 \text{ W m}^{-1}\text{K}^{-1}$ ) and neon ( $0.046 \text{ W m}^{-1}\text{K}^{-1}$ ) making it a good choice of background gas [79].

A mixture comprising mainly of a noble gas, with a small amount of a second gas of lower ionisation energy allows for easier ignition than when using a single pure gas. Such combinations of gases are known as Penning mixtures. Although using a Penning mixture would lead to a lower breakdown voltage, many successful operations of microplasmas have used pure argon [53][65][66] or helium. Stable operation of microplasma with a cavity diameter of  $13 \mu\text{m}$  has been reported in pure Ne [94]. However further reductions in the cavity dimensions may be aided by using a Penning mixture. A mixture of He and Ar, in which Argon was the more abundant, was used to create a microplasma inside a  $5 \mu\text{m}$  diameter cavity [80]. This apparent necessity for a Penning mixture is attributed to the higher number of electrons lost to the walls; a process which becomes more important on the smaller scales. Using a combination of gases helps to replace lost electrons and may be necessary for cavity diameters less than  $10 \mu\text{m}$  and pressures higher than atmospheric.

### 1.5.7 Applications

Singular microplasma devices with current with electron densities up to  $5 \times 10^{16} \text{ cm}^{-3}$  emit a high intensity of radiation the frequency of which may be varied by varying the discharge gas used [74]. Even with a fairly low ionisation rate, power consumption on the order of  $10^3 \text{ W cm}^{-3}$  are common [55]. This scale of discharge, therefore, has a much higher electron density than atmospheric plasmas (electron density values on the order of  $10^{12} \text{ cm}^{-3}$ ) [81]. Combined with their high concentration of high energy electrons, this makes microplasmas good candidates for use as light-emissive media. Grouping together many discharges into an array furthers their uses.

Arrays of many hundreds of microplasmas have been found to have a high power output for relatively low currents of a few mA when operated in parallel [66][83]. Successful operation of microplasma arrays has been achieved in a variety of materials and on a range of scales. A flexible copper-polymer-copper array has been successfully operated in air at atmospheric pressure with a lifetime of over 50 hours [82]. Another silicon based device consisting of a  $200 \times 200$  array was operated in neon at a little below atmospheric pressure [83].

The small size and minimal power input of microplasma devices makes them attractive for portable applications and a replacement for otherwise cumbersome machinery. To this end, work has been done [84] towards the use of microplasma arrays in the detection of atmospheric trace elements or compounds. Combination of an array with a gas chromatography column allows the detection of hydrocarbons to the parts per million level [85].

Further research [86][87] has been carried out on the use of microplasma arrays for the destruction of volatile organic compounds (VOCs) [88]. Passing contaminated gas through an arrays leads to the breakdown of some organic compounds and may be used for air purification, as well as environmental clean-up [66].

Excimer and ozone formation, which is favoured in microplasma devices due to high energy electrons and high pressures [89], potentially allows for the application of arrays in flat panel displays [90] and microlasers [91][72].

Further harnessing the high electron energies within discharge devices, chemical modifications have successfully been carried out by flowing molecular gases through a discharge device [92].

This offers the potential for small scale gas-phase reactors. For example, hydrogen gas was produced from a mixture of  $\text{NH}_3$  and Ar [93] with applications for a new realm of small scale portable fuel cell technology.

Several of these applications require atmospheric pressure operation, whilst others would benefit from even higher pressure operation.

Above atmospheric pressure has been reached (1.6 atmospheres) using a cathode diameter of 30  $\mu\text{m}$  [94]. In the same work, the diameter was further reduced to 13  $\mu\text{m}$  however the discharge appeared to be less stable. It is thought that this was due to the aspect ratio being larger than 1:1. Maintaining a similar ratio between cavity diameter  $D$  and electrode separation  $pd$  may be important in microplasma operation at high pressures.

It is thought that further decreasing the cathode cavity dimensions may allow operation in pressures up to 5 atmospheres or above and thus pave the way for microplasma applications in a range of physical conditions.

## 1.6 The Use of Diamond in Microplasmas

### 1.6.1 Introduction

Diamond has a giant covalent structure giving it some unique properties which often lie at the extremes of those of other materials [95][96][97]. Tetrahedrally-bonded carbon atoms join together to make up the diamond lattice [98], a unit cell of which is shown in Figure 1.18. Diamond has the face-centered cubic lattice structure, with two atoms per unit cell [99].



**Figure 1.18.** The unit cell of a diamond lattice, the black circles representing carbon atoms. *Figure taken from [100].*

As such, it has been in high demand throughout history. During the past century, much work was carried out [101] attempting to replicate the production of nature diamond and the 1950s saw commercially produced diamond realised [102]. More recently the creation of thin sheets of polycrystalline diamond films has been achieved via chemical vapour deposition (CVD) techniques, further increasing diamond's range of potential applications. This advancement has opened up the possibility of creating semiconducting diamond for use in electrical devices and as such promotes research into creating an all-diamond microplasma device.

### 1.6.2 Properties of Diamond

For microplasma applications, diamond's properties appear to be well-matched.

Table 1 highlights some of the most significant properties when considering microplasma applications. Some of the properties of diamond surfaces, such as the secondary electron emission may be changed during the fabrication process, allowing for even further modification dependent on an application's requirements [103][104].

**Table 1.** Some properties of diamond important for microplasma use [95][105]

Property	Benefit for use in microplasmas
<b>Resistant to acidic and solvent corrosion</b>	Will result in little deterioration in applications involving passing a mixture of compounds through microplasma arrays e.g. Detection of trace compounds
<b>High resistivity (<math>\approx 10^{13} \Omega \text{ cm}</math> at room temperature) therefore a good electrical insulator</b>	Aids the formation of an electric potential between electrodes
<b>High melting point (3550 ° C)</b>	Cavity walls resistant to the high temperatures of the discharge
<b>High thermal conductivity (<math>2 \times 10^3 \text{ W m}^{-1} \text{ K}^{-1}</math> at room temperature)</b>	Rapid dissipation of heat produced inside the cavity, preventing excess deterioration of the cavity of electrodes
<b>Low thermal expansion coefficient (<math>1 \times 10^{-6} \text{ K}</math> at room temperature)</b>	Reduces structural deformations due to heating
<b>Semiconductor with a band gap of 5.4 eV when doped</b>	Entire structure fabricated from a singular material reduces discontinuities at material boundaries such as electrical resistance and difference in thermal expansion
<b>Low or negative work function giving high secondary electron emission (electrons are easily expelled from diamond surfaces, with little energy input)</b>	Provides ready availability of further electrons to maintain the electron density in the discharge

The strong covalent bonds, and the rigidity of the face-centered cubic (fcc) carbon lattice (Figure 1.18) give diamond its unique properties. The tetrahedral structure of the lattice is due to the  $sp^3$  hybridised carbon atoms, whereas the  $sp^2$  hybridisation in graphite results in a planar structure [95]. This difference in bonding results in an energy barrier between the two allotropes of carbon, meaning there is no spontaneous conversion from graphite to diamond [105].

Developing successful microplasma arrays from diamond in atmospheric pressure and above promises to allow all range of applications with extremely long life times.

### 1.6.3 Doping Diamond

An insulating material, such as diamond, may be doped to become semiconducting by addition of either a higher-valence atom (n-type doping) or a lower-valence atom (p-type doping). Both work on the principle of lowering the energy required to create conducting charge carriers. A schematic representation of the energy levels in an insulating material is shown in Figure 1.19 (left). In an insulator, the energy gap between the valence and conduction band is large enough that electrons will not be excited to the conduction band on application of thermal energy. In a semiconductor however, the energy gap is smaller, meaning some proportion of electrons (dependent on the size of the energy gap) have enough energy to be excited to the conduction band [106].

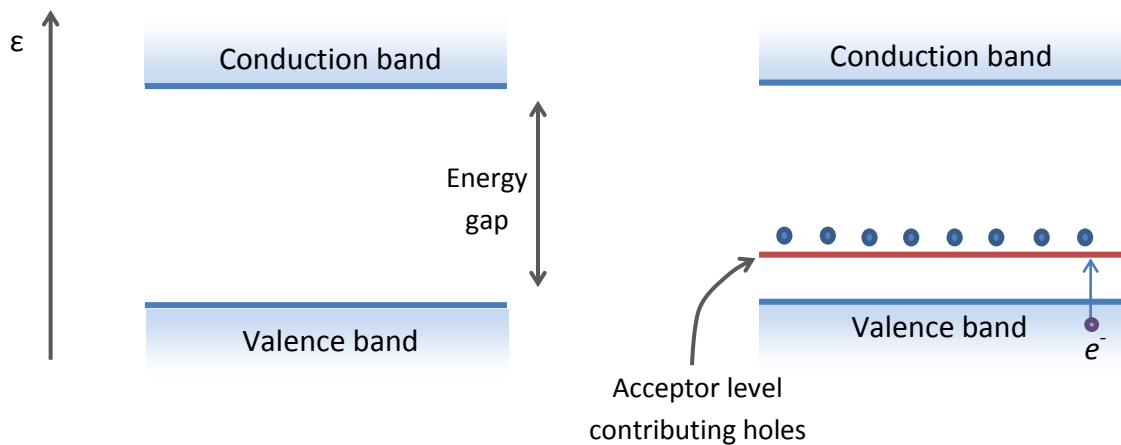


**Figure 1.19.** Diagram representing energy levels of an insulator (left) and p-type semiconductor (right). For the later, electrons move from the valence band to the acceptor level, leaving mobile holes in the valence band.

P-type semiconductors work on the principle of holes (the oppositely charged unoccupied site created by an electron on vacation of a site). Addition of a 3-valent atom (such as boron) to a 4-valent host (such as carbon) contributes acceptor impurities, or holes, to the acceptor band. Electrons from the valence band may then move into the acceptor band as the energy gap is much lower than that between the valence and conduction band. This migration of electrons creates holes in the valence band, which are mobile, and hence conducting. The concentration of acceptor impurities determines the level to which the material may become conducting [106][107][108]

Diamond may be doped to become a semiconductor with a band gap of 5.4 eV [105]. This offers the promise of creating an all-diamond device, one in which the electrodes are grown as boron-doped diamond layers. This would primarily be of an advantage in terms of the longevity of the device although secondary benefits would arise in the fabrication process, as well as the reduction of electrical junctions.

Whilst the rigid carbon lattice (Figure 1.18) gives rise to some of diamonds optical and mechanical properties, it also makes the insertion of dopant atoms difficult and atoms larger than carbon may not be incorporated easily into the lattice [105]. Boron however, being a smaller atom than carbon, may be used as a p-type dopant and incorporated into the lattice to create semiconducting diamond [109].

Layers of doped diamond for use as electrodes on either side of a microplasma device may be grown using the chemical vapour deposition technique. Where this process uses a carbon containing gas mixture (usually containing  $\text{CH}_4$ ) to deposit carbon atoms in the tetrahedral lattice arrangement,  $\text{B}_2\text{H}_6$  may be added to the mixture to produce boron-doped diamond films with boron concentrations up to  $3 \times 10^{27} \text{ m}^{-3}$  [73] [105].

The CVD process involves activation of a gas mixture which is deposited onto the required surface. The energy required to activate the gas mixture may be transmitted via different forms, such as an electrical current or a combustion flame. The process used in this project used thermal activation requiring a hot filament. A simplified version of the arrangement for this process is shown in Figure

1.20. The thickness of the b-doped film depends on the length of time for which the substrate is in the reactor [110].

Whilst it is possible to achieve near metallic conductivity, a restraint on the conductivity of the semiconducting diamond layer arises due to the polycrystalline nature of diamond fabricated using the CVD technique. The film contains cracks and grain boundaries, reducing the mobility of charge carriers [95]. The conditions for growth of high quality diamond films should therefore be employed to achieve the highest conductivity.

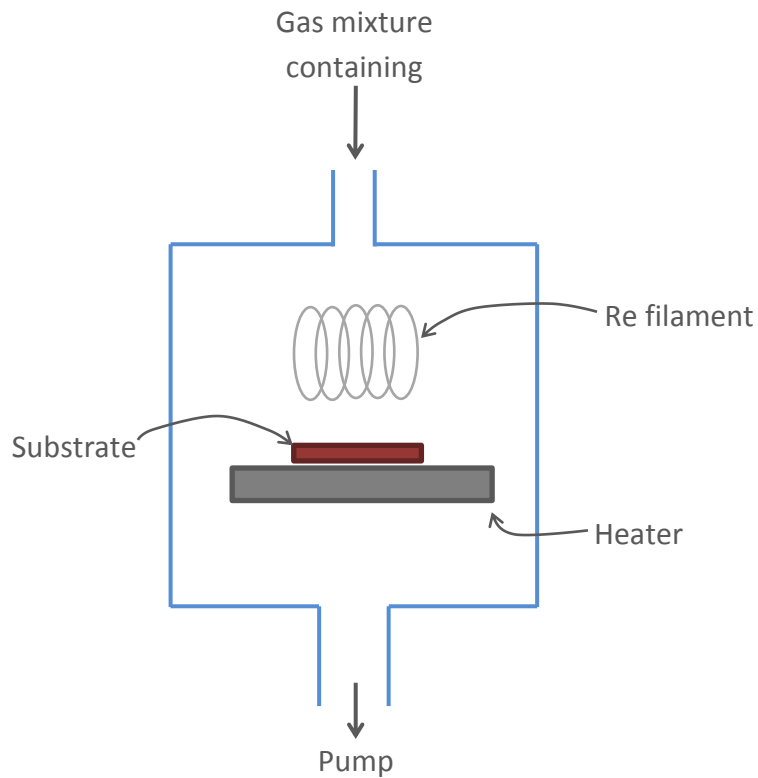


**Figure 1.20.** Schematic diagram of the hot filament reactor used to grow doped CVD diamond.

## 2 Experimental

### 2.1 Fabrication of the Devices

#### 2.1.1 The Diamond Substrate

Throughout the project several samples were created and tested, using a variety of thicknesses, electrodes and cavity diameters. The samples fabricated during this project in the laboratory were based on square microcrystalline CVD diamond wafers purchased from Element 6, which were 4.5 by 4.5 mm and 80  $\mu\text{m}$  thick. A general representation of the device is shown in Figure 2.1. Figure 2.3 A variation on this structure was created by growing a layer of semiconducting diamond on either side of the substrate using the hot-filament CVD reactor shown in Section 1.6.3. Standard conditions for CVD growth were used (a pressure of 20 Torr).  $\text{B}_2\text{H}_6$  was used as the dopant gas, and the flow rate monitored, aiming for a high enough boron concentration to give near metallic conductivity. The samples were left in the reactor for two days per side, enough to grow approximately a 3 micron layer on each side.

For both doped and undoped samples, the fabrication process was largely similar and was as follows. The first stage involved adding electrodes to either side of the substrate via a thermal deposition technique (Section 2.1.2). This was followed by creation of a cavity using a Nd:YAG laser-based micro-machining system (Section 2.1.3) and, in the case of the boron doped samples, a milling of the perimeter of the sample. The samples were then cleaned to remove graphite produced in the drilling process (Section 2.1.4).

The electrical connection was made using either gold or copper wire (both approximately 0.2 mm in diameter) and attached using a silver epoxy resin (Section 2.1.4).

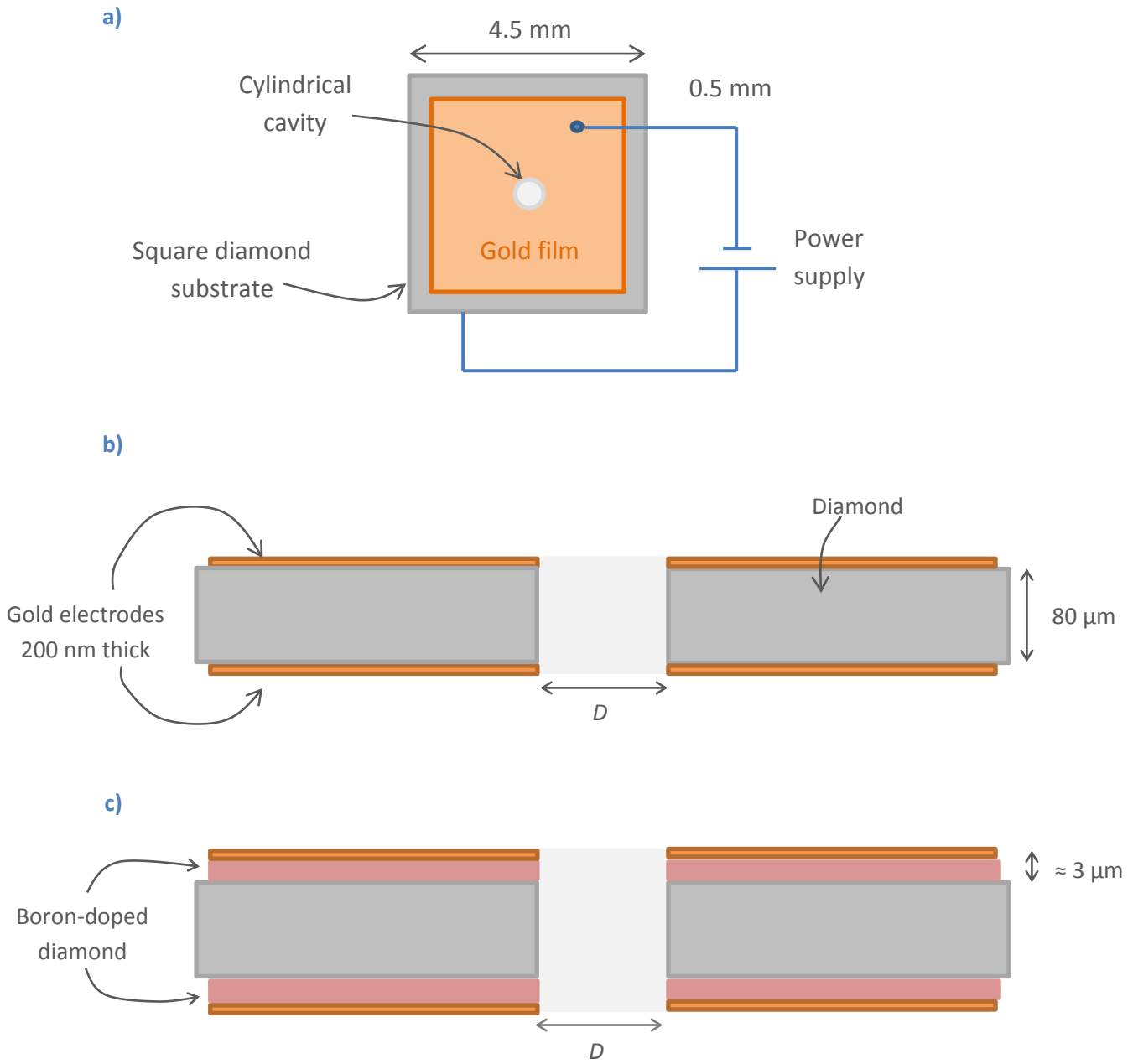


**Figure 2.1.** Simple representational diagrams of: (a) a top-down view of a gold-electrode device; (b) a cross-sectional view of a gold-electrode device; (c) a cross-sectional view of a boron-doped device with gold electrodes. *Note, diagrams are not to scale.*

### 2.1.2 Electrode Deposition

Electrodes were created by depositing a thin film of gold on either side of the sample, using a physical vapour deposition technique. The process involves creating a hot vapour of the desired deposition material in a vacuum and allowing it to condense on the desired surface. Figure 2.2 shows a simple diagram of the apparatus involved.

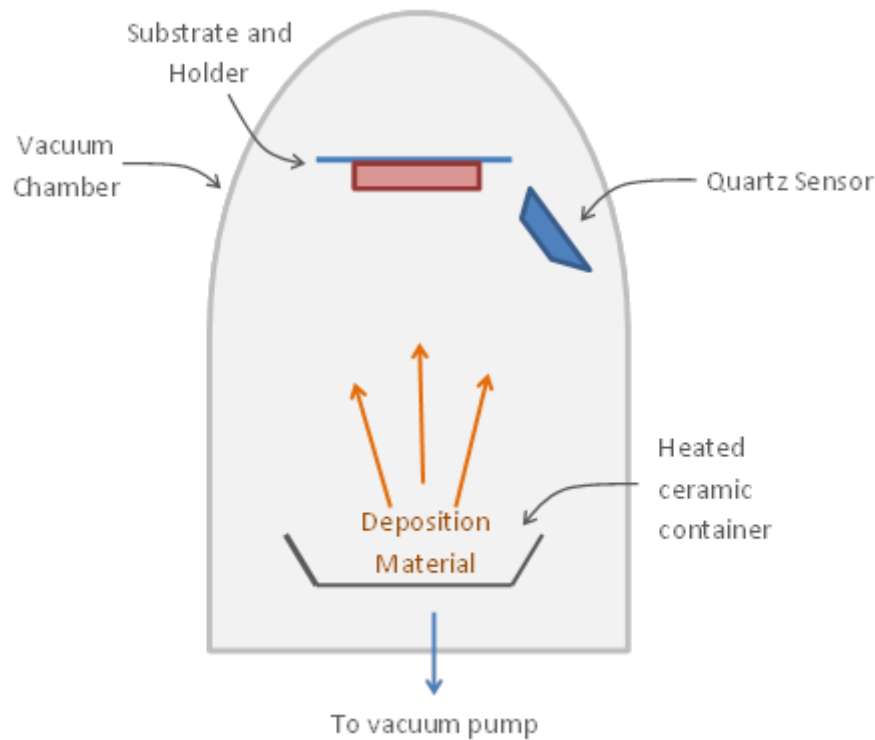


**Figure 2.2.** A simple schematic diagram of the apparatus used for physical vapour deposition using thermal evaporation.

Using a Blazer 510 machine, the diamond was first terminated with oxygen and removed of water using a 150 W air plasma at 30 mTorr for 10 minutes. Titanium was then deposited to provide an effective sticking layer at a pressure of around 10 Torr, with a thickness of approximately 10 nm, as determined by a quartz sensor. A 200nm layer of gold could then be deposited and the system pumped back to atmospheric pressure. This process enabled an even covering and thickness of the gold layer. This is an important quality for use as electrodes, where the conductivity is reduced by any defects or impurities [106] [111].

Silicon stencils, fabricated using the laser were placed over the diamond samples during Au deposition, to form a 0.5 mm border of un-coated diamond on either side of the sample (see Figure 2.1). This was important to ensure the discharge did not strike across the edges of the device when in operation.

Three samples were coated with copper electrodes when gold was not available, although the cleaning process proved difficult for these devices (see Section 2.1.4).

### 2.1.3 Laser Drilling

The cavities were created in the centre of each device using a Nd:YAG laser-based micro-machining system (Alpha, Oxford Lasers, UK). The drilling process appeared to produce a reliably cylindrical cavity, free from taper and fragmentation and of the desired dimensions.

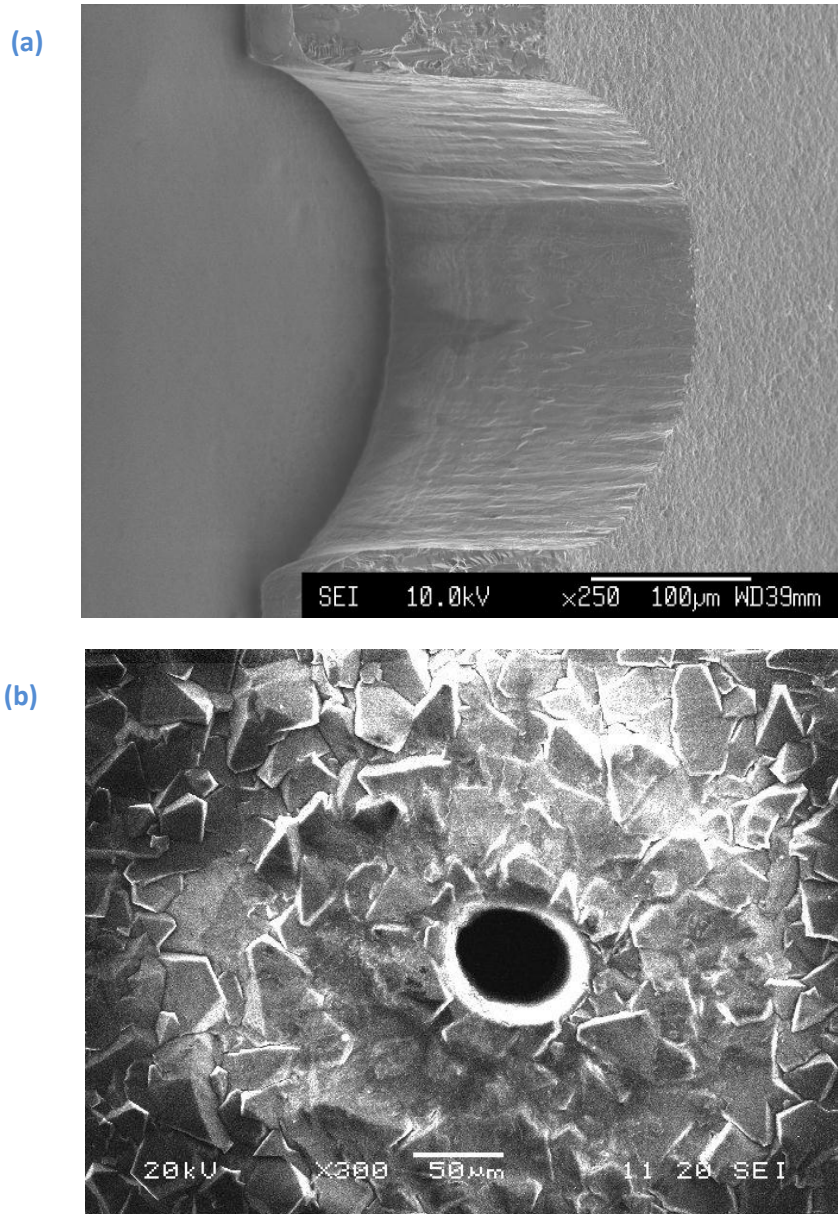


**Figure 2.3.** Image (a) shows the cross section of a 200  $\mu\text{m}$  cylindrical cavity whilst image (b) shows the end on geometry of the cavity in a polycrystalline diamond substrate. Image (a) provided from previous work by Monika Zeleznik.

As the boron-doped diamond was grown with coverage over the entire surface of the samples, it was necessary to trim the edges to ensure no semiconducting material was present on the sides of the sample. A border approximately 0.2 mm in from the edges and 4  $\mu\text{m}$  deep was also removed to ensure no shorting across the sides when in operation. This was done by using the laser on a low power (attenuator A at 20%; U at 100%) to mill to 4  $\mu\text{m}$  deep.

#### **2.1.4 Cleaning of Devices**

Laser-treating diamond surfaces has been found to produce a graphite surface layer of near metallic conductance [73][112]. As such, the process of laser-machining a cavity in a diamond substrate created a conductive pathway through the device, negating the role of the dielectric. This layer however is unstable under oxidation conditions, and therefore laser-treated samples may be cleaned with oxidising agent to remove unwanted surface impurities [112]. The presence of metallic electrodes meant harsh oxidation environments could not be used, and an appropriate cleaning process had to be chosen.

A voltmeter was used to check for electrical shorting between the top and bottom electrodes. If there was found to be little resistance, the device was cleaned using either acidic or ozone cleaning.

Due to the reactivity of gold, the usual method used to clean CVD diamond (hot sulphuric acid and potassium nitrate) [73] could not be used to clean the devices.

Nitric acid by itself however does not react with gold, although this is one of the few metals with which it does not react [113]. Warm concentrated nitric acid was therefore used to remove graphite from the gold-diamond-gold samples. This also oxygen-terminated the diamond surface [73]. It should be noted that after cleaning, the gold surface was easily scratched, and care was taken when handling the device (ceramic or plastic tweezers were used).

Three boron-doped substrates, coated with copper electrodes proved more difficult to clean due to copper's high reactivity. Instead, these devices were subject to UV radiation (at a distance of less than 5cm from the UV source) in the presence of ozone (using a UVO-Cleaner, model 42-220) for 30 minutes on each side. This method involves the excitation and dissociation of the contaminating graphite molecules by absorption of short wavelength ultraviolet radiation. Ozone is also generated, with which oxidised molecules react in order to produce more stable by-products.

This method was successful for a hole diameter of 200  $\mu\text{m}$ , however there was still conductance between the top and bottom layers after cleaning a sample with a 50  $\mu\text{m}$  cavity. The process of laser-milling the edges may have created a much larger concentration of graphite than that produced for a simple hole, or the hole itself may be too small for adequate exposure of the graphite to the ozone. It was decided that these samples would have to be recoated in gold and the nitric acid cleaning process used.

#### **2.1.5 Electrical Contacts**

For both boron-doped and undoped samples, the process of creating an electrical contact to the power supply was similar. Gold (or copper dependent on the electrode used) wires of 0.2 mm thickness were manually attached to the top and underneath side of the device, in opposite corners using a silver epoxy resin. This was cured in a 60 degree oven for 30 minutes for each contact.

Several difficulties arose during this process. Firstly, the size of the devices made avoiding the hole and edges difficult. Despite observing the samples under a microscope, and using ceramic tweezers to handle both device and wires, the area onto which the wire could be attached without

contaminating either the cavity or edges with conducting silver epoxy was small (an area of approximately  $1\text{mm}^2$ ).

Secondly, once a wire was successfully in place, extreme care had to be taken to prevent the wire becoming unstuck and moving across the device, smearing silver epoxy in the process. This made transporting the devices to the oven difficult.

Thirdly, once a wire had been successfully attached and cured, it was difficult to make the device lie flat so that the process could be easily repeated on the other side.

A solution to the second two problems was solved by placing the device on a large glass platform, rather than a singular glass slide, and using a metallic block to pin down the wire to be attached. Leaving only a couple of centimetres of wire exposed from the block allowed for a more stable attachment process and meant it was less likely to move during transport to the oven. On creation of the second contact, the previously attached wire was also pinned, and it was possible to do this in such a way that the device lay relatively horizontal.

Once both wires were attached, extreme care was needed when handling the device, as the size of the wires meant they easily broke off at the epoxy join. In attempts to ensure no other discharges were present inside the chamber, the wires were insulated using plastic tubing. This ran along the length of the wire so only the points of contact were exposed. The wires were then connected, via a washer and screw, to two metal rods which led to the external power supply (see Figure 2.4).

Two other attachment methods were tested, though neither proved more effective than the process outlined above. The first involved an air-cured silver epoxy resin, which could be applied as above and left to dry for a couple of hours. Removing the oven from the process allowed for the device and wires to be fastened in place using a sticking tape while the epoxy set, eliminating any potential movement. The necessary sections of the device could also be covered to avoid accidental contamination of the edges or hole. Unfortunately this epoxy was found to produce a weaker joint, and the wires became easily detached on application of a small force.

The second method involved using a soldering iron to provide a gluing material. Following the logic above, the idea was to eliminate the necessity of the oven in order to fasten the device in place during attachment of the wires. However it was found difficult to deposit the solder with sufficient accuracy and the idea was abandoned.

## 2.2 The High-Pressure Chamber

For testing microplasma devices, a stainless steel vacuum chamber, capable of withstanding pressures up to 10 atmospheres was connected to a vacuum pump and helium gas supply (see Figure 2.4). The chamber featured a removable platform, onto which the device could be mounted, as well as a window through which the platform could be viewed. A sandwich of sapphire plates was used to grip one edge of the device, leaving the majority of the microplasma device freely exposed to the gas in the chamber. For 80  $\mu\text{m}$  thick devices, the pinning of the sapphire sheets was modified so that they lay completely flat against each other. This was necessary in order to produce a firm hold. The pressure inside the chamber was read from a pressure gauge attached to casing of the chamber.

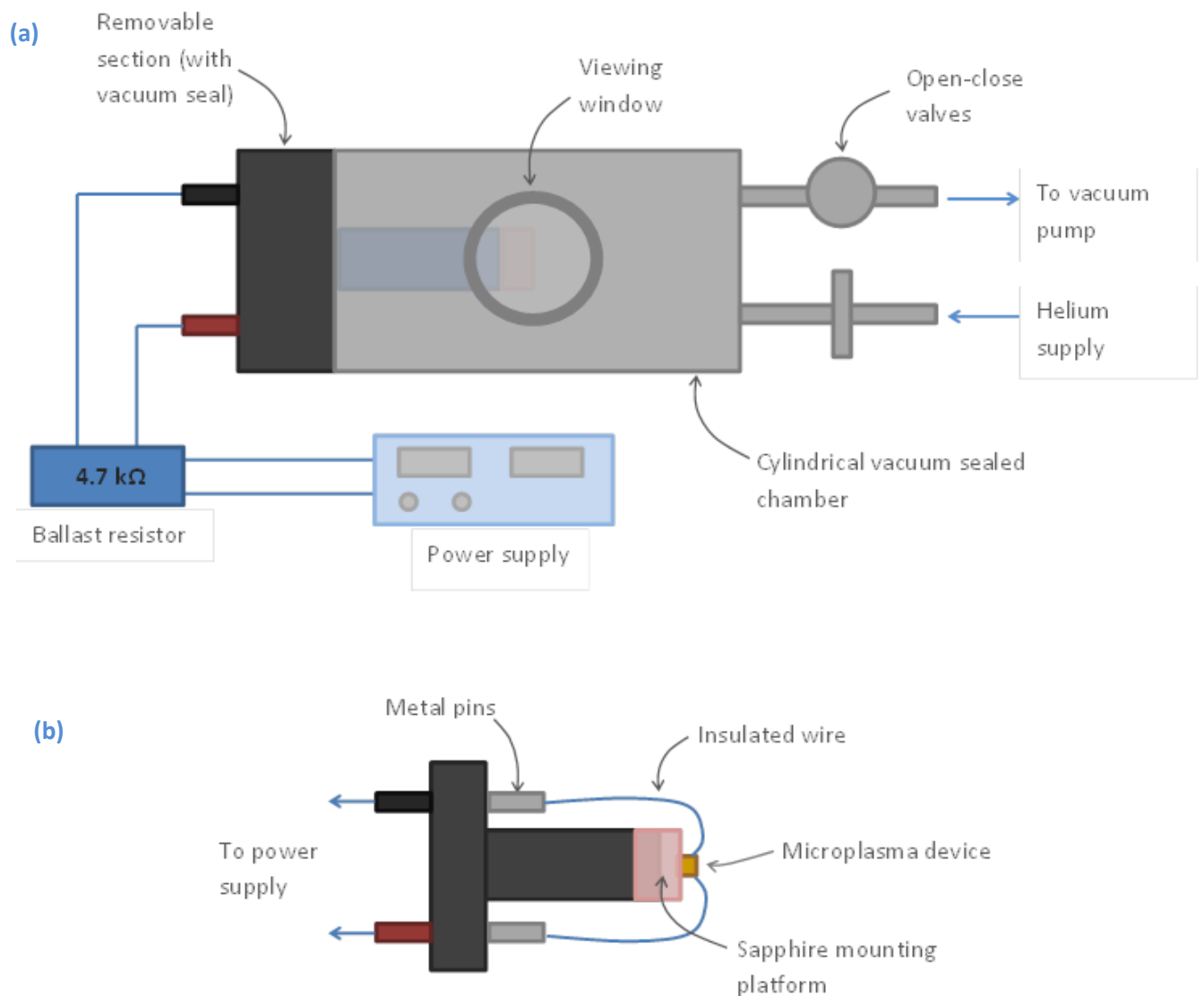


**Figure 2.4.** Schematic representation of (a) the high pressure chamber, connected to a power supply and (b) a birds-eye view of the removable section of the chamber, showing the mounting platform, and device in place with wires attached.

The device's wires could be attached to four metal pins sticking out into the chamber from the removable platform, by means of a screw and washer. The outside section of these pins could be connected to an external power source. The power source used was from Stanford Research Systems Inc. and capable of supplying up to 25 W. The voltage and current supplied to the device could then be controlled via a computer program. A limit of 3 mA was set on the current to prevent overload. Initially the voltage was raised until the discharge struck, after which the current was methodically varied in order to produce current-voltage (I-V) curves. The relationship between the voltage and current could be used to determine the mode of operation of the device, and to compare its electrical characteristics with previous works.

It was also found to be necessary to connect a ballast resistor in series with the device, in order to provide some resistance when the discharge struck, and to prevent drawing excess current. Before striking, the resistivity of the device is infinitely large, due to the insulating gap providing a capacitive effect. However this becomes almost negligible once the discharge is present inside the cavity. As current is inversely related to resistance ( $V = IR$ ) a large current is drawn, which could exceed the power supply limit, causing it to cut off. As a result, a 4.7 k $\Omega$  resistor was connected in series with the device.

### **2.3 Operation**

Once mounted with the device, the removable section of the chamber could be re-attached and the system pumped down to vacuum. The chamber was then filled with helium and pumped down to vacuum again, and the process repeated several times to ensure no air remained. The pressure could be altered by increasing the flow of helium via a needle valve and was done so in increments of 100 Torr.

To strike the discharge, the voltage was slowly increased until a sharp increase in current was observed. It was easy to check if a current rise was caused by a discharge inside the cavity by looking through the glass window.

Once struck, I-V curves were taken by increasing the current and measuring the voltage, either manually or via a computer program. A stability curve was also taken which measured the current drawn by the device. This could be left to run for several hours and produced an on-screen plot of the current against time.

Finally, a camera, which was also connected to the computer, could be used to take photographs during the device operation and was important in providing visual evidence for abnormalities in the discharge.

## 3 Results and Discussion

### 3.1 Overview

Two microplasmas were tested which produced a glow discharge; one had gold electrodes, the other was boron-doped and featured copper electrodes. A variety of further samples were created, some of which were damaged whilst some require further work in order to become operational. A summary of all outstanding samples is included in Appendix.

### 3.2 Operation of Boron-doped Sample

The pre-fabricated boron-doped sample featuring a U-shaped coating of copper was tested and a discharge was struck at 33 kPa. Despite some impurities on one surface of the device, acquired during the fabrication process, a glow discharge was produced. Figure 3.1 shows the device in operation.

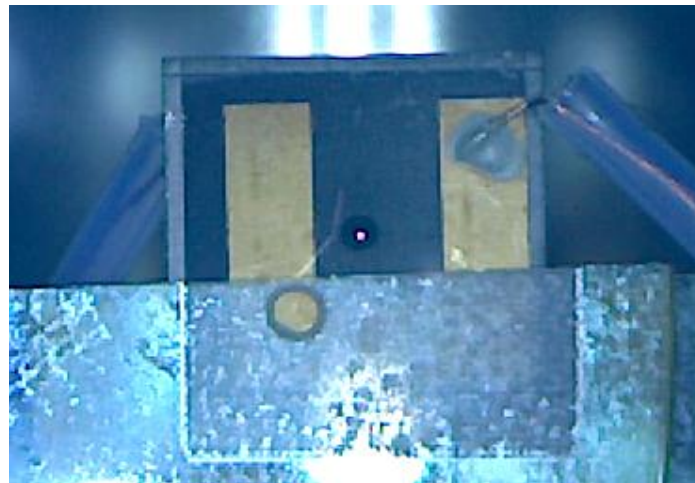


**Figure 3.1.** Image showing the discharge inside the 200  $\mu\text{m}$  cavity (in the centre of the device) during operation at 33 kPa. The photograph shows the two sides of the U-shaped copper coating, with the upper-side silver epoxy contact.

The discharge did not appear to be as bright as expected and some flickering was observed. This could have been attributed to the impurity on the surface, which was suspected to also exist inside the cavity. The sample was therefore removed for cleaning before further testing.

A second boron-doped sample was made and tested in which wires were attached directly to the semiconducting surface. It was not found possible to strike this sample. It is possible that the electrical impedance between the metal wires and the semiconducting diamond layer was too high to warrant an electrical current across the boron-doped surface and discharge across the cavity. This meant a discharge across the sides of the device became as probable as an electrical breakdown inside the hole. At high voltages (of around 700 V), a glow appeared over the entire device (Figure 3.2) rather than a localised arcing or discharge.



**Figure 3.2.** Image showing the high voltage breakdown of the helium gas around the entire boron-doped device.

As the conductance of the boron-doped layer is lower than that of the copper film [73][114] there would have been some non-zero impedance between the wire contact and the cavity hole.

Another complexity involved in doped samples is the temperature dependence of the conductance of the boron-doped layer. The conductance is proportional to the charge carrier density, which is itself proportional to temperature and it is expected that the temperature of the device will increase during operation [106]. This implies that the doped layer will have a higher conductance once the discharge is struck but may have a higher resistance prior to striking, thus raising the voltage required to create the discharge. A higher striking voltage has been observed for boron-doped electrodes compared to a metal electrode device in previous works [73].

Adding a metal layer onto which the wires may be attached would reduce the impedance due to the material boundaries. The use of a metal contact layer has produced successful discharges in 200  $\mu\text{m}$  cavities [73]. The geometry used in Figure 3.1 allows for a metal deposition on either side of the cavity in a single run. However there may be some practical difficulty in scaling the arrangement down to work on a 4.5 x 4.5 mm device or smaller. To allow for a sufficient (0.5 mm) gap around the perimeter of the sample, as well as (0.5 mm) gap for the cavity in the centre of the device, the U-shaped metal layer would have to be around 1.5mm in width. This may result in difficulties when attaching metal wires to a small target area.

### 3.3 Operation of Metal Electrode Sample

Successful operation of a metal-diamond-metal device was achieved at a range of pressures from 33 kPa (*roughly* 250 Torr) up to 132 kPa (*roughly* 988 Torr) in helium gas for over 6 hours. The discharge struck at around 270 V and operated over a current range of 0.25 – 5 mA, although this range varied with pressure.

### 3.3.1 Electrical Characteristics

Figure 3.3 shows the current-voltage plots for the highest and lowest pressure operation. The mid-range pressures have been excluded for clarity, however show much the same characteristics and may be found in Appendix. For all pressures, the I-V plots show the discharge operating with a slight negative resistivity, a characteristic which previous works have attributed towards operation in the hollow cathode mode of operation [65] (see Section 1.3.2). The minimum breakdown voltage varied with the product  $pd$  as expected of operation on the right of the Paschen minimum (

Figure 3.4. Breakdown voltage against the product  $pd$ ).

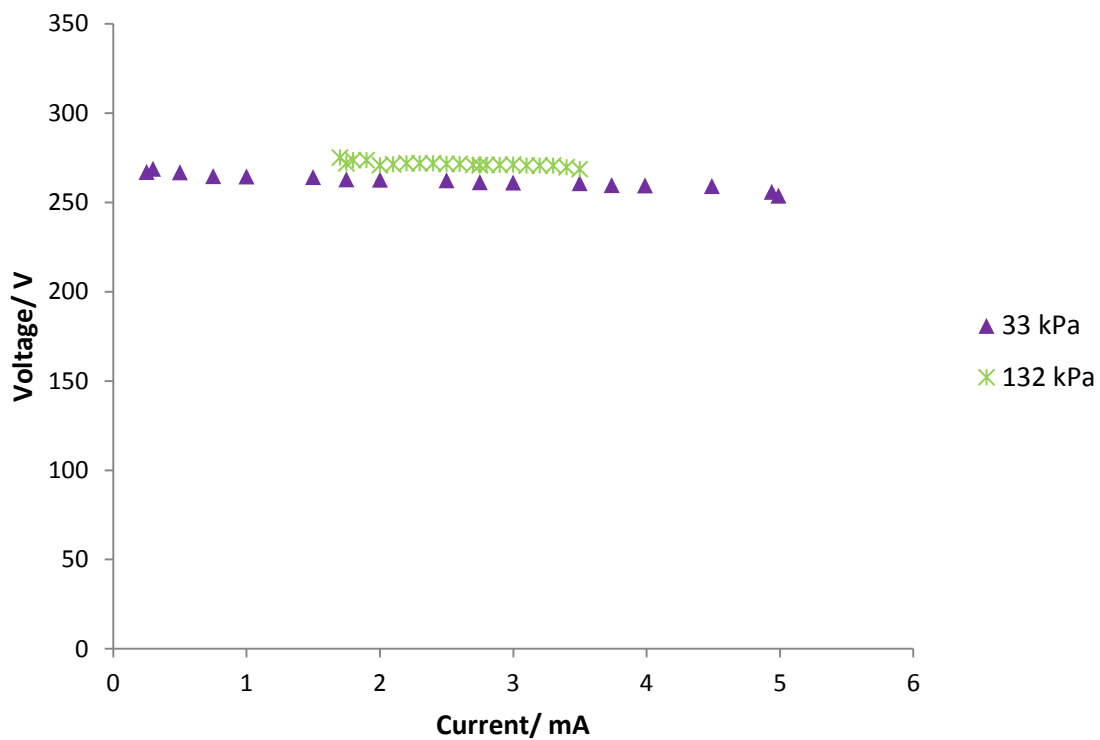
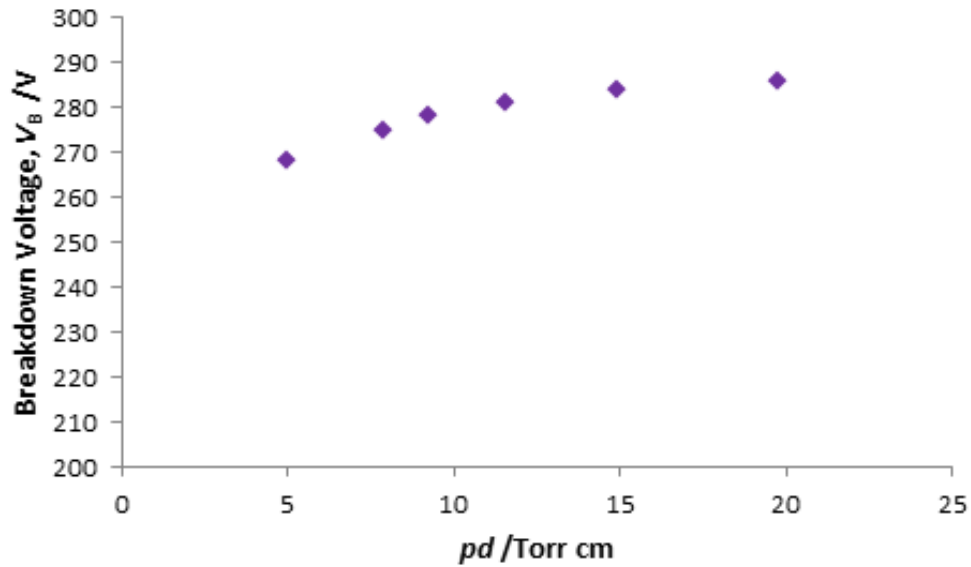


Figure 3.3. Current-voltage plots for the gold-electrode microplasma with 200  $\mu\text{m}$  cavity at the lowest and highest He pressure. The voltages have been modified to take account of the ballast resistor.



**Figure 3.4.** Breakdown voltage against the product  $pd$ .

In order to strike the device, the voltage was increased until a current was drawn. Once struck, the I-V curves were obtained by lowering the current limit and allowing the potential difference to change accordingly. A lower limit for the current was found by reducing the current limit as much as possible without the discharge extinguishing. Operation at the lower pressure (33 kPa) allowed for the lowest current (0.25 mA) whilst higher pressures became unstable around 1.5 mA. This is attributed to the higher pressure requiring a higher current density to maintain ionisation collisions [67]. It should also be noted that the current operation range is higher than noted in previous works [65][66][73][94]. This could be due to discharges elsewhere in the chamber which were not visible, or a difference in wires and electrical contacts used.

Increasing the current beyond that required for stable operation simply increased the radiation intensity from the discharge which lead to a spreading of the discharge around the cavity. This was most distinct at 132 kPa (see Figure 3.5).

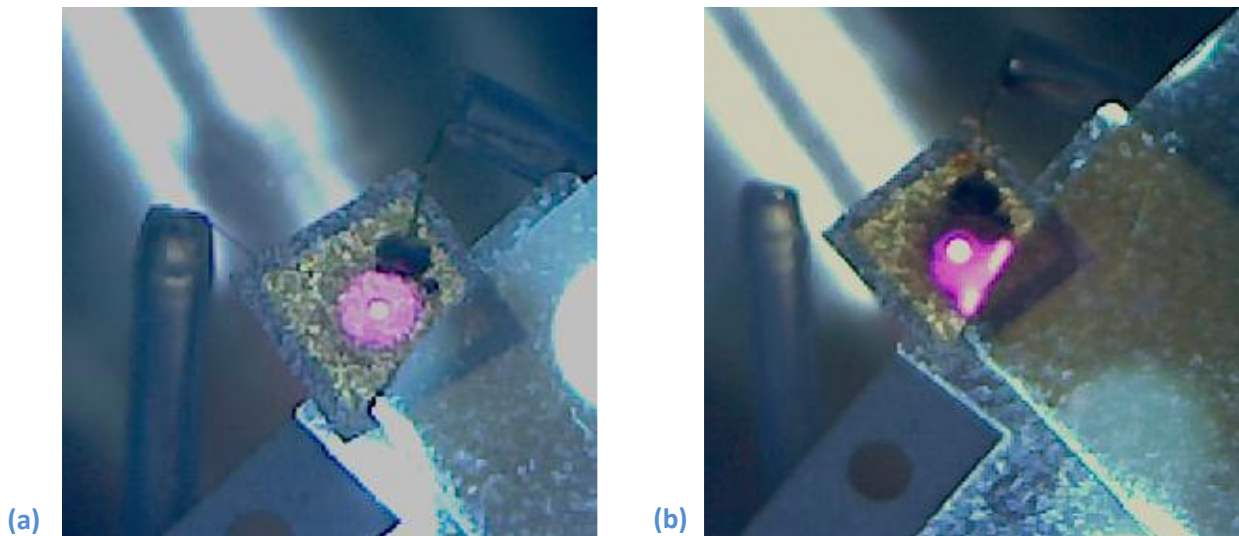


**Figure 3.5.** Image (a) showing the spreading of the discharge in a concentric circle around the cavity during normal operation and (b) during operation at 132 kPa of He for the gold electrode device with a 200  $\mu\text{m}$  diameter cavity.

Pressure increases were limited to around 100 Torr increments and were made whilst the device was in operation. On attempting a pressure increase above 1.2 atmospheres, the discharge spread further from the cavity opening. Shortly afterwards, the current dropped to zero and the discharge extinguished. There is inconclusive evidence as to whether this was as a direct result of the pressure increase, or simply the deterioration of the electrodes meaning the device had neared the end of its life. It should be noted that the aspect ratio of the device may not have favoured high pressure application. The 200  $\mu\text{m}$  cavity was intended as a test device for the fabrication process and equipment and the 80  $\mu\text{m}$  thick sheets were intended for use with lower diameter cavities.

Attempts were made to reignite the discharge, however no combination of low pressures or high voltages could make the discharge strike. SEM images (see Figure 3.7 in Section 3.3.2) suggest the conductivity of the gold electrodes was affected as a result of the spread discharge.

A stability test was carried out during which the discharge was ignited in the sample, the current set and was left to run for the remainder of the day. The current and voltage could then be checked for deviations and signs that the discharge had gone out. The values of current did not deviate however by more than 0.02 mA whilst the voltage remained stable, suggesting the stable operation of the device at low (33 kPa) pressure for over 6 hours. The glow discharge could not be left running in the laboratory overnight, however it is suspected that the discharge would have remained for more than one day at a time.

### 3.3.2 Optical Characteristics

An obvious result of altering the background gas is the change in the emission spectral lines and therefore the colour of the glow. The wavelength of light emitted is dependent on the energy gap between excited states [115] and therefore the colour of the discharge is characteristic of the background gas used. The strongest intensity wavelengths emitted in a helium atmosphere are 447

501 and 587 nm giving rise to a blue-purple glow [116]. This was the colour of the glow observed in the helium atmosphere (

Figure 3.6).

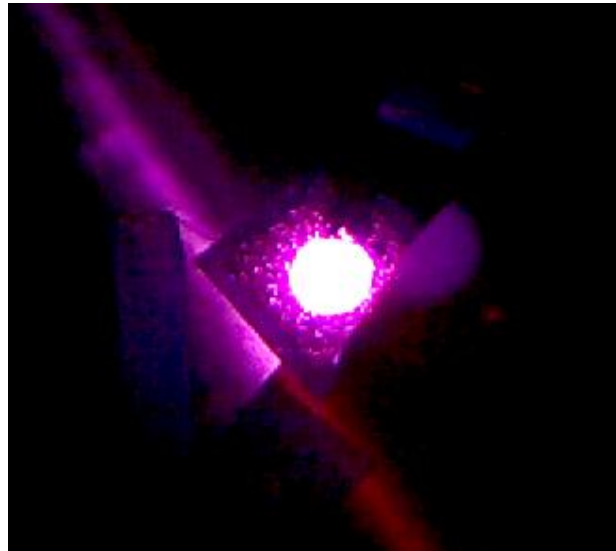


**Figure 3.6.** Image of the metal electrode device under normal operation and demonstrating the characteristic colour of excited helium gas.

Figure 3.5 (a) shows the spreading of the discharge across the circumference of the cavity and onto the electrodes. Although this is as reported in previous works [73][117], it is expected that operation with such a spreading could be detrimental for the electrodes and could be prevented with a lower operation current.

For long-term operation, the discharge should be contained so that contact with the device is limited to the diamond cavity walls. As would be expected, exposure of the gold film to the discharge resulted in its rapid deterioration. Bombardment with high energy ions and electrons resulted in sputtering of the gold surface [55]. Kinetics studies on similar microplasma devices report electrons with energies from below 1 eV to over 20 eV [47]. The energy required to remove an electron from within the bulk of a metal is given by the work function,  $\theta$ . For gold,  $\theta$  is approximately 5 eV [118]. Upon collision, the higher energy electrons present in the discharge would therefore have enough energy to ionise an electron from the gold surface. This sputtering of the gold surface leads to its degradation [119].

SEM images of the sample after operation clearly show the degradation of the gold electrodes (see Figure 3.7 (a)). In comparison, the diamond surface inside the cavity is quite smooth and shows little sign of deterioration (Figure 3.7 (c)). From the viewing chamber it is not possible to observe both sides of the device at the same time, however due to the equal amounts of gold degradation on each side, it is reasonable to conclude that the discharge looked similar at the cathode and anode. However this should be investigated and would have to be done by manually turning the removable platform around.

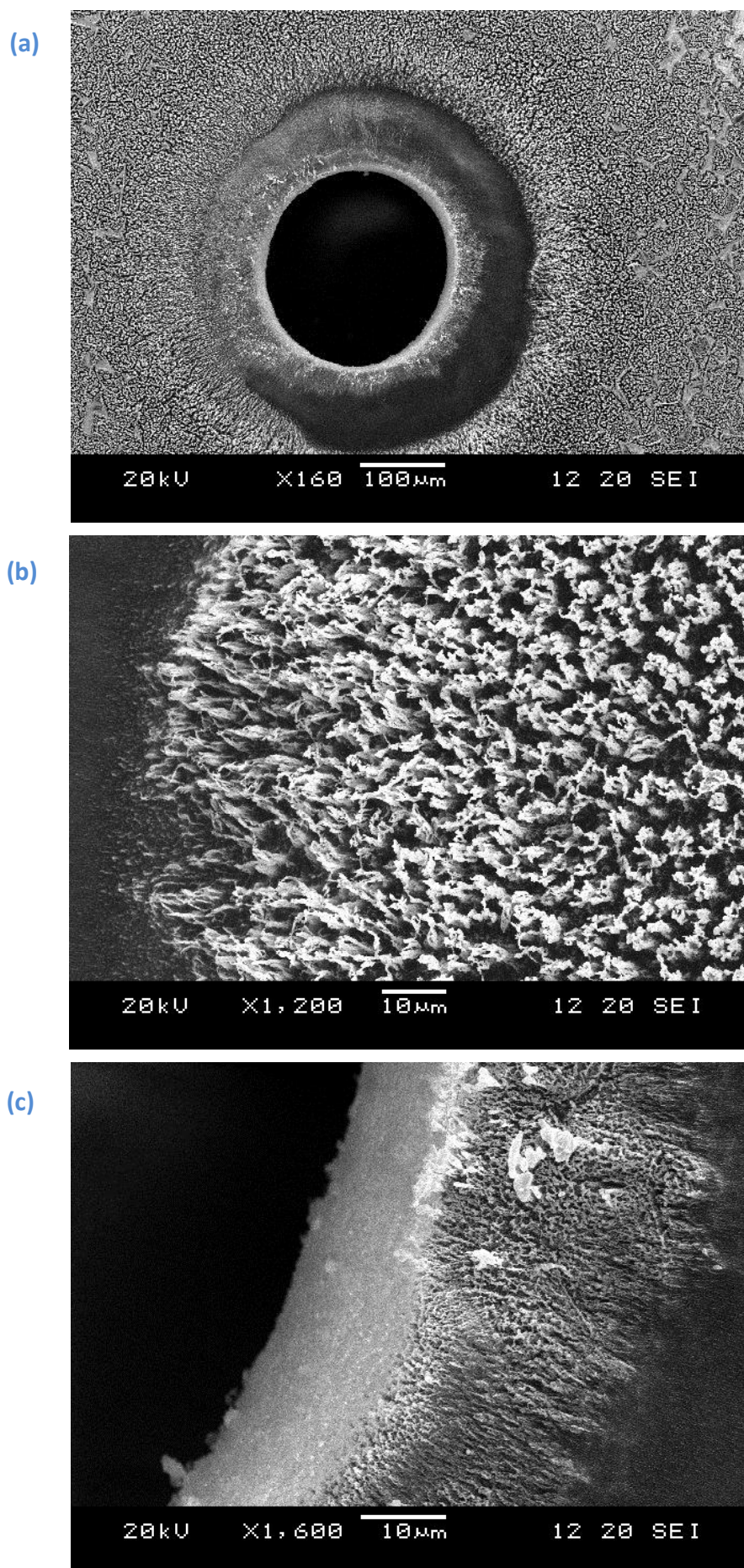


**Figure 3.7.** SEM images taken after operation and showing the destruction of the gold electrodes. Image (a) shows an area surrounding the circumference of the 200 μm cavity which appears to no longer have an Au coating. The shredding effect may be seen more closely in image (b), a stark contrast to the smooth interior of the cavity shown in image (c).

## 4 Afterword

### 4.1 Conclusion

This thesis reports the investigation into the fabrication of microplasma devices designed for operation at atmospheric pressure and above. Work during the project resulted in successful production methods of such devices as well as optimisation of the equipment necessary to carry out tests.

Successful operation of an 80  $\mu\text{m}$  thick diamond device with gold electrodes and containing a 200  $\mu\text{m}$  hole was found to be possible using the high pressure chamber and fabrication process outlined in this thesis. Operation at low pressure (33 kPa) was found possible for over 6 hours. Degradation of the gold electrodes is thought to have been a result of excess current, and it may therefore be possible to minimise this in future. Operation above atmospheric pressure was also found to be possible (132 kPa) however was not stable and the discharge extinguished rapidly. The instability is attributed to the high current and a slightly larger cavity than would normally be required for atmospheric pressure operation and above.

A discharge failed to strike in a device with wires attached directly to the boron-doped layer. It is thought that the impedance between the wires and the semiconducting layer remains too high for a current to be drawn through the cavity. However a thin metal film coating the semiconducting layer resulted in a discharge. This apparent necessity of a metal film is of important when considering how to optimise the design of an all diamond device for commercial applications. As the scale of devices decreases, and the width of the metal film layer becomes on the order of a couple of millimetres, manually attaching wires using silver epoxy resin becomes challenging.

For devices that were coated with copper electrodes, ozone cleaning for cycles of half an hour proved ineffective at removing graphite from samples with copper electrodes. This is attributed to the small dimension of the cavity and the large amount of laser machining used on these samples to removed parts of the unwanted doped layer.

Building on the process used in the Bristol Diamond lab to fabricate microplasma devices, a more flexible 0.2 mm wire was found to improve the ease of the manufacturing process when using small dimension substrates. However the flexible nature of the wires also provided a challenge. Should the top wire hang so that it rested on the edge of the device, it was likely that a discharge would strike between it and the underside electrode. Whilst plastic insulation could be used to prevent this problem in the majority of the chamber, it could not be relied upon to cover the few millimetres at the point of contact with the device. Other methods including soldering and an air-drying silver epoxy resin were tried however did not offer the strong join of the heat cured silver epoxy resin.

The method of depositing a 200 nm thick gold layer for use as an electrode proved successful, and cleaning in hot concentrated nitric acid for 25 minutes was found to remove traces of graphite without attacking the gold layer. However over-exposure did result in the peeling of the electrode layer, leaving areas stripped of gold.

While the microplasma is not subject to any amount of force once fastened inside the chamber, the method of supporting the device was found to be of importance. Two sapphire sheets held the

device firmly enough to prevent falling, but still allowed for some movement while connecting the wires to the metal pins on the inside of the removable section of the chamber. This flexibility was important as the wires would fracture at the join if put under excess stress. It was found necessary for the sapphire sheets to lie completely flat against each other at the point of inserting the microplasma; due to its 80  $\mu\text{m}$  thickness, even a small gap would prevent a sufficiently firm hold of the device.

During the course of the project, there has been no reason to believe that the fabrication process could not result in a fully operational microplasma at pressures higher than atmospheric. When handling devices of such small scale, simple processes become difficult or must be altered, however successful devices look promising, and should be achievable given a little more time.

## 4.2 Future Work

Several of the devices fabricated during the project require further work or modification before testing, but may still produce successful discharges. A table summarising the outstanding samples is included in Appendix.

As the size of microplasma devices becomes smaller, manually attaching a wire to the device becomes increasingly difficult simply due to the minimised area available onto which the wire may be attached. The insulation of the wires inside the chamber to prevent electrical shorting also becomes difficult as the size of the devices decreases. However as the target operation pressure increases, the elimination of all possible discharge surfaces becomes ever more important. There is room for optimisation of the method by which the device is connected to a power supply. Using rigid insulated wires, fixed in position inside the chamber could be one possibility. However there would have to be sufficient pressure on the device for a good enough electrical contact to be made. Spring-mounting the end section of the fixed wire may be one solution to this.

Successful fabrication of devices with 50  $\mu\text{m}$  diameter cavities and below by means of the procedure outlined in this work should, in theory, allow above atmosphere pressure operation and may prove to have an increased stability. Careful fabrication of devices similar to the metal-electrode device created in this project, with cavities of 50  $\mu\text{m}$  and below should be possible and should produce a stable discharge.

One possibility to explore is that of using CVD diamond as the substrate for a microplasma device. In theory, this should be possible and would allow the entire device to be synthesised inside the laboratory. A remaining hindrance to the electronic application of diamond thin films is the polycrystalline nature of the film and the difficulty in doping. Reducing the impurities and grain boundaries in CVD diamond films would increase the lifetime of charge carriers within the doped layers [95], thus increasing the conductivity.

Another possibility in the realm of diamond microplasma devices is that of forming an array. This may be done either by creating many cavities on a single substrate, or connecting several devices similar to those created in this project. Successful operation of microplasma arrays formed from diamond would be a promising step towards the use of microplasmas in a diverse range of

commercial applications. After successful operation of singular diamond microplasma device, there should be a real possibility of creating high density arrays.

### **4.3 Acknowledgements**

I would like to thank my supervisor, Professor Paul May, for offering me a project within the Diamond Lab and for providing suggestions and his expertise in the area. I would also like to thank my secondary assessor Dr. Neil Fox, for help with electrode deposition and for all the helpful discussions along the way. Special thanks to Monika Zeleznik, who imparted her knowledge on the fabrication process and James Smith for all the time giving technical help in the lab. Finally thanks to the whole Bristol Diamond Group, for always offering their help and making the project highly enjoyable.

## 5 References

---

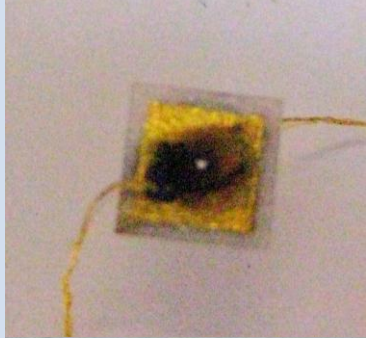
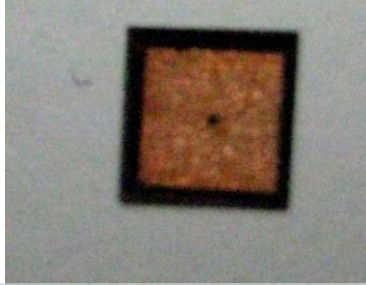
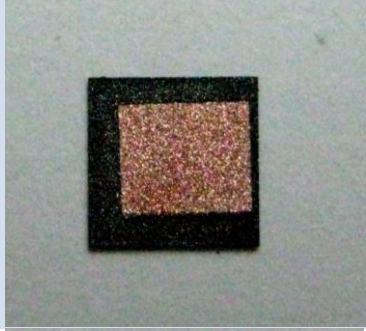
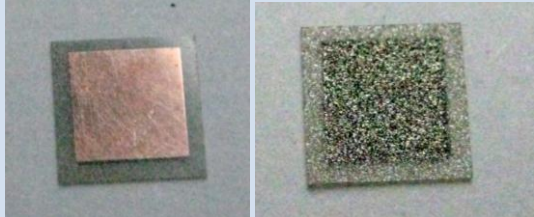
- [1] P. M. Bellan, *Fundamentals of Plasma Physics* (Cambridge University Press, 2006)
- [2] D. Gurnett and A. Bhattacharjee, *Introduction to Plasma Physics* (Cambridge University Press) 2005
- [3] G. A. Doschek, 1991, *Philos. T. Roy. Soc. A* **336** 20
- [4] A. Bogaerts, E. Neyts, R. Gijbels, J. van der Mullen, 2002 *Spectrochim. Acta B* **57** 690
- [5] D. Summers, R. Thorn, 1991 *Phys. Fluids B* **3** 1835
- [6] W. Baumjohann, R. Treumann, *Basic Space Plasma Physics* (Imperial College Press, London, 1997) p. 268
- [7] T. Cattaert, M. Hellberg, R. Mace, 2007 *Phys. Plasmas* **14** 082111
- [8] E. Dzifcakova, A. Kulinova, C. Chifor, H.E. Mason, G. Del Zanna, J. Sylwester, B. Sylwester, 2008 *Astronomy and Astrophysics* **488**
- [9] C. Tam, 1966 *Phys Fluids* **9** 3
- [10] T. J. Boyd, J. J. Sanderson, *The Physics of Plasmas* (Cambridge University Press, Cambridge 2003) Chapter 1
- [11] L. Gougam, M. Tribeche, 2011 *Phys. Plasmas* **18** 062102
- [12] P. Sturrock, *Plasma Physics* (Cambridge University Press, 1994) Chapter 2, Sections 2-3
- [13] Y. Eliezer, S. Eliezer, *The Fourth State of Matter* (IOP Publishing Ltd, Bristol, 1989)
- [14] A. Piel, *Plasma Physics: An Introduction to Laboratory, Space & Fusion Plasmas* (Springer, 2010) Chapter 11
- [15] J. Meek, J. Craggs, *Electrical Breakdown of Gases*, (Wiley, 1978) p.584 - 590
- [16] V. Cooray, *The Lightning Flash* (The Institute of Engineering and Technology, London, 2003) p. 49
- [17] D. Oxtoby, H. Gillis, A. Campion, *Principles of Modern Chemistry* (CENGAGE Learning, USA, 2008) from p.16
- [18] J. Breithaupt, *New Understanding Physics for Advanced Level, Fourth Edition* (Stanley Thornes, London, 2000)
- [19] B. Chapman, *Glow Discharge Processes: Sputtering and Plasma Etching*, (Wiley, 1980) p. 179
- [20] A. Fridman, *Plasma Chemistry*, (Cambridge University Press, USA, 2008) p.548
- [21] M. Reinicke, *Investigation of Physical and Chemical Interactions During Etching of Silicon* (Herstellung und Verlag, Germany, 2009) p.69
- [22] J. Yuan, J. Liou, *Semiconductor Device Physics and Simulation* (Plenum Press, New York, 1998) p.210
- [23] J. Meichsner, M. Schmidt, R. Schneider, H. Vagner, *Nonthermal Plasma Chemistry and Physics* (CRC Press, 2012, Florida) p.340
- [24] J. Harris, W. Benenson, H. Stocker, *Handbook of Physics* (Springer-Verlag, New York, 2002) p. 562
- [25] K. Kao, *Dielectric Phenomena in Solids* (Elsevier Academic Press, London, 2004) p.555-556
- [26] J. Meichsner, M. Schmidt, R. Schneider, H. Vagner, *Nonthermal Plasma Chemistry and Physics* (CRC Press, 2012, Florida) p.98
- [27] F. Paschen, 1916 *Ann. Phys.* **50** 901
- [28] U. Flender, K. Wiesemann, 1995 *Plasma Chem Plasma P* **15** 123-157
- [29] W. Boyle, F. Haworth, 1955 *Phys. Rev. B* **101** 935
- [30] M.J. Druyesteyn, F.M.Penning, 1940 *Rev. Mod. Phys.* **12** 87
- [31] G. Lister, 1992 *J. Phys. D: Appl. Phys* **25** 1649
- [32] A. M. Howatson, *An Introduction to Gas Discharges*, Second Edition (Pergamon Press, Surrey, 1976)
- [33] J. Williams, J. Kung, Y. Chen, X. Cai, S. Griffin, 1995 *Appl. Spectrosc* **49** 1705-1714
- [34] A. Walsh. 1956, *Spectrochim. Acta* **7** 108
- [35] A. Guntherschulze, 1923 *Z. Tech. Phys.* **19** 49
- [36] D. Goebel, K. Jameson, R. Watkins, I. Katz, I. Mikellides, 205 *J. Appl. Phys* **98** 113302
- [37] G. Schaefer, K.H.Schoenbach, *Physics and Applications of Pseudosparks* (Plenum, New York 1990)
- [38] D. J. Sturges, H. J. Oskam, 1964 *J. Appl. Phys.* **35** 2887
- [39] R. Sankaran, K. Giapis, 2002 *J. Appl. Phys.* **92** 5
- [40] K.Schoenbach, 1998 *Bull. Am. Phys Soc.* **43** 1478
- [41] F. Paschen, 1916 *Ann. Phys.* **50** 901
- [42] F.M. Penning, *Electrical Discharges in Gases* (Macmillan & Co. Ltd, 1965)
- [43] M.A Lieberman, A.J.Litchenberg, *Principles of Plasma Discharge* (John Wiley and Sons Inc. New Jersey 2005)
- [44] A. D. White, 1959 *J. Appl. Phys.* **30** 711
- [45] J. W.ewartowski, H. A. Watson, *Principles of Electron Tubes* (Van Nostrand, Princeton, NJ, 1965) p. 561.
- [46] A. El-Habachi, K. Schoenbach, 1998 *Appl. Phys. Lett.* **72** 22
- [47] J. Choi, F. Iza, J.K. Lee, C.Ryu, 2007 *IEEE Trans. Plasma Sci.* **35** 1274
- [48] H. Uhm, E. Choi, G. Cho, J. Ko, 2000 *J. Appl. Phys.* **64** 275-285

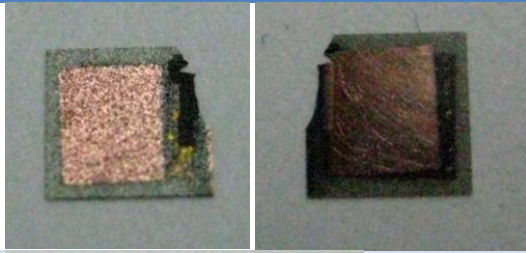
- 
- [49] E. Munoz-Serrano, G. Hagelaar, T. Callegari, J. Boeuf, L. Pitchford, 2006 *Plasma Phys. Control. Fusion* **48** 391-397
- [50] P. Kisliuk, 1959 *J. Appl. Phys.* **30** 51
- [51] H. Chang, C. Ryu, S. Yoo, S. Kim, S. You, 2012 *J. Phys. D: Appl. Phys.* **45** 195206
- [52] R. Stark, K. Schoenbach, 1999 *Appl. Phys. Lett.* **74** 3770
- [53] D. Spasojevic, V. Stefleková, N. Sisovic, N. Konjevic, 2012 *Plasma Sources Sci. Technol.* **21** 025006
- [54] L. Boeuf, L. Pitchford, 1993 *Surf. Coat. Tech* **59** 32-40
- [55] M. Kushner, 2005 *J. Phys. D: Appl. Phys.* **38** 1633
- [56] S. 56kawa *et al*, 2012 *J. Phys. D: Appl. Phys.* **45** 253001
- [57] K. Schoenbach, R. Stark, 1999, *J. Appl. Phys.* **85** 2075
- [58] A. Yahya, J. Harry, 1999 *Int. J. Electron.* **86** 755-762
- [59] J. Greenan, C. Mahony, D Mariotti, P. Maguire, 2011 *Plasma Sources Sci. Technol.* **20** 025011
- [60] R. Tirumala, D. B. Go, 2010, *Appl. Phys. Lett.* **97** 151502
- [61] A. Wallash, L. Levit, 2003 *Proc. Of SPIE* **87** 183
- [62] D. Go, D. Pohlman, 2010 *J. Appl. Phys.* **107** 103303
- [63] W. Boyle, P. Kisliuk, 1955 *The Physical Review* **97** 2
- [64] A. Phelps, 2001 *Plasma Sources Sci. Technol.* **10** 329-343
- [65] K. Schoenbach, A. El-Habachi, W. Shi, M. Ciocca, 1997 *Plasma Sources Sci. Technol.* **6** 468-477
- [66] K. Becker, K. Schoenbach, J. Eden, 2006 *J. Appl. Phys.* **39** R55-R70
- [67] L. Boeuf, L. Pitchford, K. Schoenbach, 2005, *Appl. Phys. Lett* **86** 071501
- [68] P. Kurunczi, H. Shah, K. Becker, 1999 *J. Phys. B: At. Mol. Opt. Phys.* **32** L651-L658
- [69] I. Petzenhauser, L. Biborosch, U. Ernst, K. Frank, K. Schoenbach, 2003 *Appl. Phys. Lett.* **83** 4297
- [70] P. von Allmen, D. Sadler, C. Jensen, N. Ostrom, S. McCain, 2003 *Appl. Phys. Lett.* **82** 4447
- [71] H. Park, T. Lee, K. Park, H. Baik, 2003 *Appl. Phys. Lett.* **82** 3191
- [72] P. von Allmen, S. McCain, N. Ostrom, B. Vojak, J. Eden, F. Zenhausern, C. Jensen, M. Oliver M, 2003 *Appl. Phys. Lett.* **82** 2562
- [73] S. Mitea, M. Zeleznik, M.D. Bowden, P.W. May, N.A. Fox, J.N. Hart, C. Fowler, R. Stevens and N. StJ. Braithwaite, 2012 *Plasma Sources Sci. Technol.* **21**
- [74] S. Park, J. Eden, J. Chen, C. Liu, J. Ewing, 2001 *Opt. Lett.* **26** 1773
- [75] J. Chen, S. Park, Z. Fan, J. Eden, C. Liu, 2002 *J. Microelectromech. S.* **11** 536
- [76] R. Block, O. Toedter, K. Schoenbach, 1999a *Proc. 30th AIAA Plasma Dynamics and Lasers Conf. (Norfolk, VA, July 1999)* Paper AIAA-99-3434
- [77] R. Block, M. Laroussi, F. Leipold, K. Schoenbach, 1999b *Proc. 14th Int. Symp. on Plasma Chemistry (Prague, Czech Republic, August 1999)* vol 2, p 945
- [78] A. Fridman, L. A. Kennedy, *Plasma Physics and Engineering* (Taylor & Francis, New York, 2004) Chapter 4, p. 202
- [79] N. B. Vargaftik, *Handbook of Thermal Conductivity of Liquids and Gases* (CRC Press Inc, 1994)
- [80] T. Kim, E. Kim, S. Park, J. Eden, 2011 *IEEE T. Plasma Sci.* **39** 11
- [81] S. Samukawa *et al*, 2012 *J. Phys. D: Appl. Phys.* **45** 253001
- [82] S. Park, C. Wagner, C. Herring, J. Eden, 2000 *Appl. Phys. Lett* **77** 199
- [83] J. Eden, S. Park, N. Ostrom, K. Chen, 2005 *J. Appl. Phys D: Appl. Phys* **38** 1644-1648
- [84] M. Miclea *et al* 2002, *Proc. Hakone VIII (Puehajaerve, Estonia)* p. 206
- [85] K. Kunze, M. Herring, J. Eden, 2006 *Appl. Phys. Lett.* Submitted
- [86] A. Koutsospyros, S-Y. Yin, C. Christodoulatos, K. Becker, 2004 *Int. J. Mass Spectrom.* **233** 305
- [87] A. Koutsospyros, S-Y. Yin, C. Christodoulatos, K. Becker, 2005 *IEEE Trans. Plasma Sci.* **33** 42
- [88] K. Urashima, J. Chang, 2000 *IEEE T. Dielect. El. In.* **7** 5
- [89] P. Kurunczi, K. Martus, K. Becker, 2003 *Int. J. Mass. Spectrom.* **223/224** 37
- [90] K. Choi, 1999 *IEEE Trans. Electron Devices* **46** 2256
- [91] K. Schoenbach, M. Moselhy, W. Shi, R. Bentley, 2003 *J. Vac. Sci. Technol. A* **21** 1260
- [92] D. Hsu, D. Graves, 2003 *J. Phys. D: Appl. Phys.* **36** 2898
- [93] H. Qiu, K. Martus, W. Lee, K. Becker, 2004 *Int. J. Mass. Spectrom.* **233** 19
- [94] S. Park, J. Eden, 2002 *Appl. Phys. Lett.* **81** 4127

- 
- [95] M. Ashfold, P. May, C. Rego, N. Everitt, 1994 *Chem. Soc. Rev.* **23** 21-30
- [96] J. Field, *The Properties of Natural and Synthetic Diamond* (Academic Press, 1992) p.474
- [97] J. Holman, P. Stone, *Chemistry* (Nelson Thornes Ltd, Cheltenham, 2001) p.88
- [98] H. Pierson, *Handbook of Carbon, Graphite, Diamond and Fullerenes: Properties, Processing and Applications* (Noyes Publications, 1993)
- [99] L. Pan, *Diamond: Electronic Properties and Applications* (Kluwer Academic Publishers, USA, 1995) p. 3
- [100] O. J. L. Fox, 2011 *Deposition of nanocrystalline diamond films by MW plasma CVD & Gas-Phase diagnostics using in-situ molecular-beam mass spectrometry and emission spectroscopy*, PhD Thesis, Department of Chemistry, University of Bristol
- [101] J. Hershey, *The Book of Diamonds: Their Curious Lore, Properties, Tests and Synthetic Manufacture* (Kessinger Publishing LLC, 2004)
- [102] P. Bundy, T. Hall, M. Strong, R. Wentorf, 1995 *Nature* **176** 4471
- [103] C. Bandis, B. Pate 1995 *Phys. Rev. B* **52** 12056–71
- [104] A. Shih, J. Yater, C. Hor, R. Abrams, 1997 *Appl. Surf. Sci.* **111** 251–8
- [105] P. W. May (2000), *Phil. Trans. R. Soc. Lond. A* **358** 473-495
- [106] C. Kittel, *Introduction to Solid State Physics, Eighth Edition* (John Wiley & Sons, USA, 2005)
- [107] H. Ibach, H. Luth, *Solid State Physics – An Introduction to Principles of Materials Science, Fourth Edition* (Springer-Verlag, Germany, 2009)
- [108] Professor Walther Schwarzacher, 2013 *Physics of Semiconductors and Magnetism Course*, School of Physics, University of Bristol
- [109] A. T. Collins, A. W. S. Williams, 1971 *J. Phys. C: Solid State Phys* **4** 1789
- [110] P.W. May, N.M.Everitt, C.G. Trevor, M.N.R. Ashfold, K. N. Rosser, 1993 *Appl. Surf. Sci.* **68** 299-305
- [111] M. Aguilar, A. I. Oliva, P. Quintana, 1998 *Surf. Sci.* **409** 501-511
- [112] S. M. Pimenov *et al*, 1993 *Diam. Relat. Matter* **2** 291-297
- [113] T. R. Dulsky, *A Manual for the Chemical Analysis of Metals*, (American Society for Testing and Materials, Ann Arbor, MI, 1996) Chapter 3
- [114] N. R. Wilson, S. L. Clewes, M. E. Newton, P. R. Uwin, J. V. Macpherson, 2006 *J. Phys. Chem. B* **110** 5639-5646
- [115] G. F. Knoll, *Radiation Detection and Measurement, Fourth Edition* (Wiley, Hoboken, N.J. 2010)
- [116] F. A. Jenkins, H. E. White, *Fundamentals of Optics, Fourth Edition* (McGraw-Hill, 1976) Chapter 21
- [117] K. H. Schoenbach, R. Verhappen, T. Tessnow, F. E. Peterkin, W. W. Byszewski, 1996 *Appl. Phys. Lett.* **68** 13
- [118] P. A. Tipler, R. A. Llewellyn, *Modern Physics, Third Edition* (W.H. Freeman, New York, 1999)
- [119] R. V. Stuart, *Vacuum Technology, Thin Films and Sputtering: An Introduction* (Academic Press, New York, 1983)

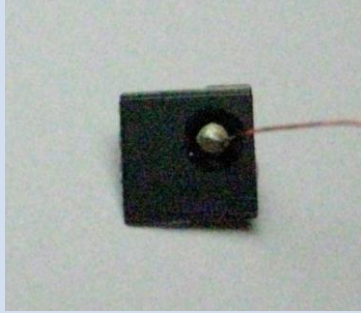
## Appendix

**Table 1.** A photographic summary of samples created or tested during the project, including a brief description and further action, if any.

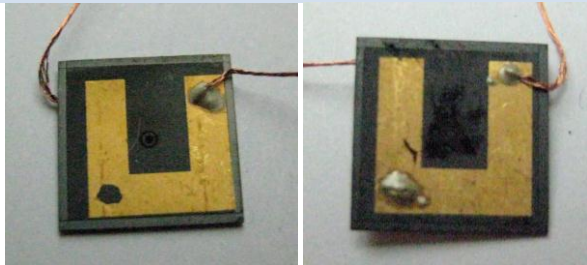
Microplasma Device	Description and Suggested Further Action
	<ul style="list-style-type: none"> <li>• <b>M101</b> 80 <math>\mu\text{m}</math> thick diamond substrate, 200 <math>\mu\text{m}</math> cavity; 200 nm thick Au electrodes; Gold wires attached</li> <li>• <b>Tested (Section 3.3) and successfully struck, however no longer strikes.</b></li> </ul>
	<ul style="list-style-type: none"> <li>• <b>B101</b> 80 <math>\mu\text{m}</math> thick diamond substrate; 50 <math>\mu\text{m}</math> cavity; Cu electrodes; Edges milled to 4 <math>\mu\text{m}</math> deep</li> <li>• <b>Cannot be cleaned in UVO cleaner – suggest removing copper electrodes and replacing for gold</b></li> </ul>
	<ul style="list-style-type: none"> <li>• <b>B102</b> 80 <math>\mu\text{m}</math> thick diamond substrate; Cu electrodes; No milled edges or cavity</li> <li>• <b>Cannot be cleaned in UVO cleaner – suggest removing copper electrodes and replacing for gold</b></li> </ul>
	<ul style="list-style-type: none"> <li>• <b>B103</b> 80 <math>\mu\text{m}</math> thick diamond substrate; Cu electrodes; Two edges milled on crystalline side (darker appearance)</li> <li>• <b>Cannot be cleaned in UVO cleaner – suggest removing copper electrodes and replacing for gold</b></li> </ul>
	<ul style="list-style-type: none"> <li>• <b>M102</b> 80 <math>\mu\text{m}</math> thick diamond substrate; Cu film on one side (left), Ti coating on other (right)</li> <li>• <b>Suggest acid clean and re-deposition of Au electrodes</b></li> </ul>



- **M103** 80  $\mu\text{m}$  thick diamond substrate; Cu electrodes; Chip on corner – milled edge to prevent contact over sides
- **Suggest acid clean and re-deposition of Au electrodes**



- **S102<sup>119</sup>** 80  $\mu\text{m}$  thick diamond substrate; 80  $\mu\text{m}$  diameter hole; boron doped layers; wires attached directly to doped layers (one wire fell off); Tested but failed to strike
- **Acid clean to remove epoxy, add metal electrode or contact**



- **B104** 200  $\mu\text{m}$  thick diamond substrate; 200  $\mu\text{m}$  diameter cavity; boron doped layers; U-shaped copper contacts; Discharge struck successfully (although dimly)
- **Remove impurity around cavity (right)**

